Central Arctic Ocean surface-atmosphere exchange of CO_2 and CH_4 constrained by direct measurements

John Prytherch[1,2,3], Sonja Murto[1,3], Ian Brown[4], Adam Ulfsbo[5], Brett F. Thornton[3,6], Volker Brüchert[3,6], Michael Tjernström[1,3], Anna Lunde Hermansson[7], Amanda T. Nylund[7], Lina A. Holthusen[8*]

[1]Department of Meteorology, Stockholm University, Stockholm, 10691, Sweden
[2]Department of Earth Sciences, Uppsala University, Uppsala, 75236, Sweden
[3]Bolin Centre for Climate Research, Stockholm, 10691, Sweden
[4]Plymouth Marine Laboratory, Plymouth, PL1 3DH, United Kingdom
[5]Department of Marine Sciences, University of Gothenburg, Gothenburg, 40530, Sweden
[6]Department of Geological Sciences, Stockholm University, Stockholm, 10691, Sweden
[7]Department of Mechanics and Maritime Sciences, Chalmers University of Technology, Gothenburg, 41296, Sweden
[8]Chemical Oceanography Department, GEOMAR Helmholtz Centre for Ocean Research Kiel, Kiel, 24105, Germany
* now at: Institute for Chemistry and Biology of the Marine Environment, University of Oldenburg, Oldenburg, 26129, Germany

Correspondence to: John Prytherch (john.prytherch@misu.su.se)

Abstract. The Central Arctic Ocean (CAO) plays an important role in the global carbon cycle, but the current and future exchange of the climate-forcing trace gases methane (CH_4) and carbon dioxide (CO_2) between the CAO and the atmosphere is highly uncertain. In particular, there are very few observations of near surface gas concentrations or direct air-sea CO_2 flux estimates, and no previously reported direct air-sea CH_4 flux estimates from the CAO. Furthermore, the effect of sea ice on the exchange is not well understood. We present direct measurements of the air-sea flux of CH_4 and CO_2, as well as air-snow fluxes of CO_2 in the summertime CAO North of 82.5 N from the Synoptic Arctic Survey (SAS) expedition carried out on the Swedish icebreaker *Oden* in 2021.

Measurements of air-sea CH_4 and CO_2 flux were made using floating chambers deployed in leads accessed from sea ice and from the side of *Oden*, and air-snow fluxes determined from chambers deployed on sea ice. Gas transfer velocities determined from fluxes and surface water dissolved gas concentrations exhibited a weaker wind speed dependence than existing parameterisations, with a median sea-ice lead gas transfer rate of 2.5 cm hr^{-1} applicable over the observed 10-m wind speed range (1-11 m s^{-1}). Average observed air-sea CO_2 flux was -7.6 mmol m^{-2} day^{-1}, and the average air-snow CO_2 flux -1.1 mmol m^{-2} day^{-1}. Extrapolating these fluxes and the corresponding sea-ice concentrations gives an August and September flux for the CAO of -1.75 mmol m^{-2} day^{-1}, within the range of previous indirect estimates.

Average observed air-sea CH_4 flux of 3.5 μmol m^{-2} day^{-1}, accounting for sea ice concentration, equates to an August and September CAO flux of 0.35 μmol m^{-2} day^{-1}, lower than previous estimates and implying that the CAO is a very small, << 1%, contributor to the Arctic flux of CH_4 to the atmosphere.

1 Introduction

The Arctic is on average warming up to 4 times faster than the global average rate (Rantanen et al., 2022), manifested in dramatic reductions in sea-ice extent (Onarheim et al., 2018) and thickness (Kwok, 2018). Reduced sea-ice cover in a warming Arctic is expected to have complex effects on air-sea gas exchanges (Parmentier et al., 2013), in particular for the exchange of the two gases whose rising atmospheric concentrations are principally responsible for the observed global warming, carbon dioxide (CO_2) and methane (CH_4). The parameterisation of gas transfer in the presence of sea ice is still under debate but is expected to have large impacts on polar carbon budgets: for example, Arctic Ocean CO_2 uptake estimates are highly dependent on the parameterisation choice, with resulting uptake differences of 50 Tg C yr^{-1}, ~30 % of the total (Yasunaka et al., 2018). The Arctic Ocean corresponds to 5-14% of the global ocean CO_2 sink from 3% of the global ocean area (Bates and Mathis, 2009; Yasanuka et al., 2016; Yasanuka et al., 2018).

The Central Arctic Ocean's (CAO) role in carbon cycling and exchange of climate-forcing trace gases with the atmosphere is uncertain due to several factors, including limited observations of dissolved gas concentrations and air-sea fluxes. The CAO is defined as the deep-water part of the Arctic Ocean, excluding the shallow shelf seas (Jakobsson, 2002). Thus defined, the CAO has an average depth of 2748 m and an area of 4.5 x 10^6 km^2, which corresponds to about 47% of the surface area of the entire Arctic Ocean.

Sources of CH_4 from the Arctic Ocean are poorly constrained and spatially variable (Thornton et al., 2016a). Oceans have long been seen as generally a weak source of CH_4. The shelf seas of the Arctic and particularly the extensive shallow East Siberian Shelf are believed to be a large source, though are poorly constrained. Here, with potential sources of CH_4 from thawing subsea permafrost and riverine input (Weber et al., 2019; Manning et al., 2020), fluxes of 9-286 μmol m^{-2} day^{-1} were observed with direct measurement (Thornton et al., 2020), and 187-238 μmol m^{-2} day^{-1} were estimated from seawater concentrations (Thornton et al., 2016b). While the integrated magnitude of these Arctic marine methane emissions remains under debate, it appears to presently be on the scale of ~4-5 Tg CH_4 yr^{-1} or 100 μmol m^{-2} day^{-1} (Thornton et al., 2016a; 2016b; 2020), ~1% of global CH_4 emissions (Saunois et al., 2020). There are previously no direct CH_4 flux measurements available from the CAO. The estimates that are available are derived from near-surface (typically ~ 10 m depth) concentrations (Manning et al., 2022; Damm et al., 2018; Fenwick et al., 2017; Lorenson et at., 2016). Seawater CH_4 measurements from the North American Arctic shelf and Canada Basin suggest small fluxes, 0.3 – 2.2 μmol m^{-2} day^{-1} (Manning et al., 2022; Fenwick et al., 2017). Excess CH_4 may be transported from shallow sea areas across the Arctic Ocean in the water column and also frozen in sea ice and in brines within the ice (Damm et al., 2018). Seawater CH_4 concentrations from the Beaufort Shelf and CAO were used to estimate an Arctic-wide CH_4 flux of 7.5 μmol m^{-2} day^{-1}, and a potential flux, if the ice would disappear from currently ice-covered areas, of 18-63 μmol m^{-2} day^{-1} (Lorenson et al., 2016). Emissions of CH_4 derived from changing seawater concentrations following a winter storm ~150 km north of Svalbard were 19 μmol m^{-2} day^{-1} during and 5 μmol m^{-2} day^{-1} afterwards (Silyakova et al., 2022). Much higher fluxes, 125 μmol m^{-2} day^{-1}, extending for at least 50 km over wintertime (November and April) sea-ice leads at latitudes up to 82°N, have been derived from aircraft-based atmospheric profile

measurements (Kort et al., 2012). These fluxes, observed over deep water, are ascribed to local CH_4 production associated with the mixed sea ice and lead environment. The large range of indirect estimates of CAO CH_4 emissions presents a challenge to modeling and highlights the need for direct measurements.

The CAO is generally undersaturated with respect to atmospheric CO_2. This undersaturation is due to a combination of the low temperatures and resulting lower gas saturation, dilution due to freshwater input, limited atmospheric equilibration due to the presence of sea ice, $CaCO_3$ dissolution (Fransson et al., 2017), vertical mixing and primary production, particularly in shelf seawater advected to central areas (Bates et al., 2006). Average Arctic Ocean uptake in summer months, with sea-ice concentration (SIC) of ~50% and a CO_2 partial pressure (pCO_2w) undersaturation of ~ 80 μatm, is estimated at -4 mmol m^{-2} day^{-1} (Yasunaka et al., 2018). The majority of existing Arctic Ocean observations are from coastal regions, with average air-sea fluxes in the Eastern Arctic Ocean 0 –10 mmol m^{-2} day^{-1} (Manizza et al., 2019) and average air-sea fluxes in the Western Arctic Ocean somewhat higher, 0 – 20 mmol m^{-2} day^{-1}, primarily due to low SIC in the Chukchi Sea (Bates and Mathis, 2009; Ouyang et al., 2022). In the CAO, observations of pCO_2w and the air-sea flux are especially sparse. Yasunaka et al., (2018), using a self-organising map to extrapolate the sparse near-surface CO_2 observations, determine the mean flux for the CAO region to be below the uncertainty of their method (uncertainty 2.8 to 3.7 mmol m^{-2} day^{-1}). Coupled ocean-biogeochemistry modelling gives an annual CAO flux of -2.2 ± 4.0 Tg CO_2 yr^{-1} (Manizza et al., 2019). Earlier estimates from the Canada Basin suggested fluxes smaller than -3 mmol m^{-2} day^{-1} in periods with SIC near 100%, but an uptake of around -55 mmol m^{-2} day^{-1} in summer months, with lower SIC (Bates et al., 2006). High fluxes can occur when water undersaturated with CO_2, high winds and open water coincide, with CO_2 fluxes up to -86 mmol m^{-2} day^{-1} estimated in June close to the pack edge north of Svalbard (Fransson et al., 2017). Fluxes determined from direct, eddy covariance, measurements in areas adjacent to ice or from lead water surfaces are of the order of -10 mmol m^{-2} day^{-1}, in both central and coastal areas of the Arctic Ocean (Prytherch et al., 2017; Dong et al., 2021; Prytherch and Yelland, 2021).

The presence of sea ice makes the Arctic Ocean a highly heterogenous and dynamic environment over a wide range of spatial scales, complicating robust model representation of surface exchange processes. Wind speed is the primary forcing of gas exchange in the ice-free ocean (Wanninkhof et al., 2009). Sea ice limits air-sea gas exchange, but also contributes to its forcing through additional sea-ice dependent physical processes that impact interfacial mixing. This implies a non-linear relationship of gas transfer rate to sea-ice cover (Loose et al. 2014). The highest rates of gas exchange in pack ice regions occur through open water areas such as leads. Leads appear on scales from < 1 m to > 10 km, and can open, change size and close throughout all seasons (Marcq and Weiss, 2012). Sea-ice dependent processes impacting gas exchange from lead surfaces are: shear between floating ice and the underlying water (Lovely et al. 2015); upper ocean stability, stratification from freshwater during ice melt and convection-driven turbulent mixing from surface buoyancy during freeze periods (MacIntyre et al. 2010). Also, modifications to the wind stress input from ice-edge form drag, ice-wave interactions and short fetch conditions (Bigdeli et al. 2018). Direct ship-based eddy covariance measurements support an inverse linear scaling of exchange with SIC (Butterworth & Miller, 2016; Prytherch et al. 2017) while laboratory and indirect radon isotope measurements support an enhanced exchange (Fanning & Torres, 1991; Loose et al. 2011; 2017). Recent direct and indirect gas exchange observations

suggest that gas exchange will be reduced in the presence of sea ice (Rutgers van der Loeff et al. 2014; Prytherch and Yelland, 2021).

Strong, near-surface gradients in dissolved gas concentrations are prevalent in Arctic sea-ice regions (e.g. Miller et al., 2019; Ahmed et al., 2020; Dong et al., 2021). Unaccounted for, this stratification will bias flux estimates and parameterisations of gas transfer derived from sub-surface concentrations. Using eddy covariance (EC) flux measurements, Dong et al. (2021) showed that surface fCO_2 in the summertime Arctic marginal ice zone was 39 μatm lower than that measured from their ship's intake at 6 m depth. They determined that this was partly due to effects on CO_2 solubility from meltwater cooling and freshening, with approximately half of the reduction from other factors, presumably photosynthesis. Miller et al. (2019) report pCO_2w differences between the surface and an intake at 7 m depth of between -180 and +160 μatm during sampling in the Canadian Arctic Archipelago and Hudson Bay. The authors note that "The temperature differences between the underway system and the shallower samples were often contrary to the pCO2 gradients…, indicating that pCO2 was not simply controlled by surface heating and cooling". Due to surface longwave emission and the resulting cool skin effect (Woolf et al., 2016), temperature differences are always present between the sea surface and intake depths even when the upper ocean is well mixed.

Sea-ice can be porous due to brine channels within the ice and can exchange gases with the atmosphere (Delille et al. 2014). Ice-atmosphere fluxes of CO_2 are typically smaller than those through water surfaces, on the order of 1 mmol m^{-2} day^{-1}, but can be a significant contributor to regional fluxes in sea ice areas. Ice-atmosphere fluxes are largely dependent on temperature (Delille et al., 2014) and snow cover thickness (Geilfus et al., 2012; Nomura et al., 2010). Ice-atmosphere CH_4 fluxes are less well known. Sea ice cores obtained on the Siberian shelf have been supersaturated with CH_4, while cores from the CAO were close to equilibrium, but atmospheric fluxes were not determined (Damm et al., 2015). There are no reported measurements of ice-atmosphere CO_2 or CH_4 flux in the summertime CAO.

The high sensitivity and small footprint of the flux chamber technique makes it attractive for measurements in small water bodies such as leads. The technique has been frequently used in inland water bodies but is criticised because the chamber isolates the air-water interface from the wind and may modify the gas exchange process. While this isolation suggests that chambers reduce gas transfer, previous studies have often suggested an overestimation of k when determined from chambers, resulting from artefact turbulence at the water surface introduced by the chamber, particularly at very low wind speeds (Matthews et al., 2003; Vachon et al., 2010). The gas transfer of poorly soluble gases is controlled by mixing on the water side of the interfacial layer, and the mixing itself depends on forcings such as wind speed (Wanninkhof et al., 2009). If water is able to advect into the chamber rapidly and with minimal modification by the chamber, then the gas transfer within the chamber will be representative of the outside environment. Appropriate chamber designs with minimal penetration into the water layer, high surface to volume ratios, and short measuring intervals minimize such measurement bias.

To remedy some of the uncertainties reviewed above we here report direct measurements of the air-sea flux of CO_2 and CH_4, gas transfer velocities determined from the air-sea flux measurements and surface water dissolved gas concentrations,

and air-snow fluxes of CO_2 during the period of rapid sea-ice melt in the summertime CAO. We relate the gas transfer velocities to wind speed and lead width, discuss the measurement uncertainties and estimate regional CAO fluxes.

2. Methods

Measurements were obtained during the Synoptic Arctic Survey (SAS) expedition (Snoeijs-Leijonmalm et al., 2022) carried out on the Swedish icebreaker *Oden* in 2021. The science operations of the expedition began on August 1, when *Oden* reached the ice edge north of Svalbard (80.71°N, 11.20°E). Oden transited to the North Pole along 30°E, then towards the northern coast of Greenland along the Lomonosov Ridge, then East from the Morris Jesup Rise towards Svalbard, with relevant science operations finishing on September 11 (Fig. 1, Fig. 2a).

Ice stations were carried out throughout the expedition during which *Oden* halted in the ice for periods ranging between several hours and 2 days in order to perform winch operations such as Conductivity Temperature Depth sensor and Niskin bottle casts and net deployments. During long-duration stations, sampling was carried out directly from the sea ice at locations within a radius of ~200 m of *Oden*, or to a radius of ~500m using *Oden's* helicopter. During shorter stations where on-ice work was not possible, measurements were performed from over the side of the ship (overside).

2.1 Gas flux measurements

Measurements of air-water CO_2 and CH_4 flux were made using floating chambers (e.g., Cole et al., 2010). Two types of floating chamber sampling were performed: ice-based sampling, with the chamber placed onto lead water or meltpond surfaces accessed from sea ice and allowed to float freely; and overside sampling during the shorter stations, with the chamber lowered over *Oden's* side to the water surface, resulting in sampling closely adjacent to the ship. Fluxes measured overside may be influenced by the presence of *Oden* impacting the gas exchange rate both through modification of the near-surface winds and through modification of ocean near-surface turbulence. Measurements were made as far from any propellor movement or water flushing as possible but there may still have been some influence on the measurements. In the presence of upper-ocean dissolved gas concentration gradients, mixing induced by *Oden* may modify the air-sea concentration difference that drives the flux. As such, overside and ice-based flux and surface water gas concentration measurements are presented separately throughout this study.

Two floating chamber flux systems were used during SAS, both comprising a gas analyser and air pump connected through tubing in a closed loop with the chamber. The first system used a Los Gatos Research (LGR) Greenhouse Gas Analyser cavity-enhanced laser spectrometer, measuring mixing ratios of CO_2, CH_4 and H_2O. The second system used a Li-COR 7200RS non-dispersive infrared (NDIR) spectrometer, measuring CO_2 and H_2O mixing ratios. Surface fluxes of a gas species are determined from the gradient with time of the gas mixing ratio in the chamber, with an approximately linear gradient required for a successful flux measurement. The sampling time for each flux measurement was approximately 10 minutes, after which the chamber was manually raised from the surface and equilibrated with atmosphere, before being

replaced to begin the next sampling period. Each chamber deployment during SAS typically consisted of ~8 sampling periods (from 2 to 10). The mean of the fluxes measured within each deployment is used in the subsequent analysis, with the standard error of fluxes indicating the variability within each deployment. Fluxes were converted to mmol m^{-2} day^{-1} using the chamber surface area, the volume of the total chamber system (chamber, tubing, and analyser measurement cell), chamber air pressure and the ideal gas law.

The same chambers were used with both analysers. The chambers are custom built, consisting of upturned polyethylene bowls, with foam floats attached and rubber stoppers in the roof through which the tubing is inserted (Supplemental Materials Fig. S1). The chambers are lightweight, low profile (volume 7489 ml, surface area 0.078 m^2), have small chamber wall intrusion depths (< 3 cm) and are allowed to float freely. Wind is the dominant source of surface mixing energy in the open ocean and most large water bodies. Chamber flux measurement necessarily involves isolation of an area of water from the wind. The chamber design and sampling choices are made to minimise known measurement biases resulting from anchoring effects (Lorke et al., 2015), and from chamber size and shape and sampling duration (Matthews et al., 2003; Mannich et al., 2019). Similar chamber designs to that deployed here have been shown to determine gas exchange rates in agreement with those determined in streams and small lakes from tracer releases (Cole et al., 2010), surface dissipation measurements and IR imagery (Gålfalk et al., 2013). With appropriate flux chamber design (i.e., the relatively small and lightweight chambers used here) it is assumed that the wind-induced interfacial layer mixing, the controlling factor for air-sea gas transfer of poorly soluble species, is advected within the chamber with minimal modification of the mixing by the chamber.

Air-snow CO_2 flux measurements were made using a PP systems CPY-4 chamber connected to an EGM-4 NDIR analyser and mixed by a fan inside the chamber (e.g. Miller et al. 2015). The transparent chamber (volume 2344 ml, surface area 167 cm^2) was covered to minimise insolation effects, and deployed on undisturbed snow surfaces. The chamber collar was pressed 1 cm into snow to prevent air leaks. The sampling time was also 10 minutes here.

Measurements of surface atmosphere CO_2 and CH_4 flux were also made throughout the expedition by EC from a system installed on *Oden's* foremast (Prytherch et al., 2017). Post-cruise analysis determined that fluxes measured in sea-ice regions were below the limit of detection of this system. While the strong observed CO_2 undersaturation resulted in air-sea fluxes at the lead spatial scale that would be within the typical detectable range of EC systems, the high sea-ice concentration within the EC footprint (of approximately km^2 scale from the 20 m EC measurement height) throughout the expedition substantially reduced the signal size (e.g. Prytherch et al., 2017), and as such EC measurements are not used in the analysis here (see Supplementary Material).

Throughout this manuscript we use the convention that positive fluxes are upwards, i.e., indicating a release of gas from the surface to the atmosphere, and negative fluxes are a downwards flux, indicating uptake of gas by the surface from the atmosphere.

2.2 Water sampling

Onboard *Oden,* an underway seawater intake system continuously pumped water from a depth of approximately 8 m. Water temperature at 8 m depth was measured close to the underway line inlet with 2 hull contact sensors, and the temperature and salinity of the underway line water was measured using a Seabird SBE45 thermosalinograph (TSG) located in *Oden's* main lab. Downstream of the TSG on the underway line, a Pro Oceanus CO_2-Pro CV membrane equilibration sensor measures equilibrated CO_2 mixing ratio from which pCO_2w was calculated. This sensor was factory-calibrated prior to the expedition and performed an automated zeroing procedure every 6 hours. The manufacturer states the accuracy to be ± 3 ppm.

Surface water was sampled during the expedition to determine dissolved gas concentrations and carbonate system variables. Water samples were taken using bottles submerged at depths of 0-10 cm and using syringes at depths of 0-5 cm. During some stations a Ruttner sampler was used to obtain water samples at depths from 0.5 to 2.5 m. During overside chamber flux sampling, water samples were obtained using a lowered bucket, with the resulting water depth range for bottle and syringe samples corresponding approximately to the height of the bucket (0 – 30 cm). Temperature and practical salinity during each sampling were measured with a WTW 340i conductivity probe. Discrete sampling at depth and from the underway line followed the washing and repeat overflow protocols described in Dickson et al. (2007). For surface water bottle sampling, the bottles were first washed with seawater then submerged by hand gradually while lying sideways to minimise air-water mixing as it was not possible to follow standard overfilling protocols (Dickson et al., 2007). Syringe sampling is not described in the carbon system sampling protocols, but follows Bastviken et al. (2003). The syringes were repeatedly washed with seawater prior to sampling.

Samples of dissolved inorganic carbon (DIC) and total alkalinity (TA) were collected in Pyrex® borosilicate bottles (250 ml) according to Dickson et al. (2007), without being poisoned with mercury chloride ($HgCl_2$). Samples were stored short-term (typically less than 12 hours, +4°C and dark) and thermostated to 25°C in a water bath prior to analysis. DIC was determined using a coulometric titration method based on Johnson et al. (1987) with a modified Single Operator Multiparameter Metabolic Analyzer (SOMMA) system (coulometer type UIC 5012) and the mean difference and standard deviation of duplicate sample analysis were 5.0 ± 2.5 μmol kg^{-1} (n=12). TA was determined using a semi-open cell potentiometric (Orion ROSS 8102BN) titration (Metrohm Dosimat 665) method using a 5-point Gran evaluation (Haraldsson et al., 1997) and the mean difference and standard deviation of duplicate sample analysis were 3.4 ± 2.5 μmol kg^{-1}. The accuracy in DIC and TA was ensured by routine analysis of certified reference material (CRM Batch #181 and #191) obtained from A. G. Dickson of Scripps Institution of Oceanography (La Jolla, CA, USA). The pCO_2w was calculated from measured DIC and TA using the CO2SYSv1.1 MATLAB toolbox (Lewis and Wallace, 1998; van Heuven et al., 2011) and the dissociation constants of Lueker et al. (2000).

Samples for CH_4 analysis from surface leads, buckets, CTD and the pumped underway line were collected into 500 ml borosilicate bottles. Bottles were allowed to overfill with the bottle volume three times to remove gas bubbles, poisoned with 100 μl of saturated $HgCl_2$, then transferred to the laboratory. Prior to analysis, samples were placed into a water bath at

25°C and thermostated for a minimum of two hours before analysis. All samples were analysed within 3 days of collection. Samples were analysed by single-phase equilibration gas chromatography (GC)using a flame ionisation detector (FID), similar to that described by Upstill-Goddard et al. (1996). Samples were calibrated against three certified ±5% reference standards which are traceable to NOAA WMO-CH4-X2006A. Concentrations in seawater at equilibration temperature (~25°C), in situ salinity, and dissolved partial pressures of CH_4, pCH_4w, were calculated using the ideal gas law, Henry's law and CH_4 solubility determined by Wiesenburg and Guinasso (1979).

Additional water samples were collected with 60 ml PVC plastic syringes, where 30 ml of seawater was equilibrated with 30 ml air immediately after sampling, and the equilibrated air sample stored as headspace in 20 ml vials that were prefilled without headspace with saturated NaCl solution (Bastviken et al., 2003). The headspace gas was analysed after the expedition using the methods described in Lundevall Zara et al. (2021) and determined on an SRI 8610 GC with FID and methanizer. Headspace concentrations were corrected for the atmospheric background of CH_4 and CO_2 determined with the LGR gas analyser, accounting for the soluble fraction in the equilibrated 30 ml water sample, and pCO_2w and pCH_4w calculated. The precision of replicate equilibration samples was 5 % or better.

For each sampling time and location, the bottle- and syringe-derived measurements were combined to obtain an average time series of both surface pCH_4w and surface pCO_2w. with measurement uncertainty given as the standard error of the mean (the range between the bottle and syringe values is equivalent to twice the standard error). A comparison of the measurements obtained from the different sampling methods and further details of the averaging process is given in Supplementary Material section 1 and Fig S2.

2.4 Meteorological and sea-ice measurements

Meteorological measurements were made onboard *Oden* using a semi-permanent suite of instrumentation (Vüllers et al., 2021). Wind speed and direction was measured on the foremast at 20 m height, corrected for airflow distortion (Prytherch et al., 2017) and adjusted to 10 m height assuming a logarithmic profile and neutral stability conditions, which are prevalent in the summertime CAO. For winds coming from behind *Oden* (more than 90° from bow on), mast measurements were replaced with those from anemometers mounted at each side of the bridge roof at 28 m height, also corrected for height but not airflow distortion. All wind measurements are given as ice-relative speeds. Air temperature and humidity were measured on the foremast at 20 m height with aspirated sensors. Surface temperature was determined as the average measurement of two KT15.IIP infrared sensors mounted on each side of the bridge roof at 25 m, observing the surface approximately 30 m to port and starboard of *Oden's* hull. Snow and ice surface temperatures were additionally measured adjacent to snow/ice flux sampling using thermistors inserted into the upper few cm of the snow or ice surface. Lead widths and other distances were measured with a laser rangefinder (Naturalife PF4). Sea-ice thickness and freeboard were determined adjacent to ice flux sampling sites as the average from three 2-cm auger-drilled holes.

Surface buoyancy flux into lead waters was determined following MacIntyre et al. (2009) using the net radiative fluxes and turbulent heat fluxes made onboard *Oden* (Vüllers et al., 2021) and water surface temperature and salinity. Turbulent fluxes were gap-filled using the bulk estimates (Smith, 1988).

2.5 Gas transfer velocity calculation

The air-sea flux, F_X, of a poorly soluble gas species X, such as CO_2 and CH_4, can be represented as (e.g., Wanninkhof et al., 2009; Fairall et al., 2022):

$$F_X = kK_{0X}\Delta f_X, \quad (1)$$

where K_{0X} is the aqueous phase solubility of X (mol m^{-3} atm^{-1}) and Δf_X is the difference in the fugacity of X between the surface water and air. Fugacity is partial pressure corrected for non-ideality: this correction is very small (< 1%) for CO_2 and CH_4 in summertime Arctic conditions (McGillis et al., 2006), and partial pressures are used in all calculations reported here. The gas transfer velocity, k, represents the kinetic forcing of the flux, dependent on both molecular diffusivity, D, water viscosity, ν, and processes that impact transfer across the water surface interfacial layer. To account for the dependence of diffusivity on gas species, temperature and salinity, k is commonly normalised in terms of the non-dimensional Schmidt number Sc ($Sc = \nu/D$:

$$k_{660} = k, \quad (2)$$

here 660 is the Schmidt number of CO_2 in seawater at 20°C and the exponent n depends on the hydrodynamics of the interfacial layer, and is commonly chosen to be 0.5 for a wavy surface (e.g., Jähne et al., 1987).

We determine k_{660} from Eqs. (1) and (2) using measurements of F_X from the floating chamber, measured partial pressure differences, and solubilities and Sc calculated from the polynomial relationships summarised in Wanninkhof (2014), with the solubility relationships for CO_2 and CH_4 originally determined by Weiss (1974) and Wiesenburg and Guinasso (1979) respectively. Uncertainties in k_{660} are determined from combination of the flux and surface water partial pressure standard errors. Where the partial pressure comprised only one sample and so had no error value, the mean partial pressure standard error for that species is used instead.

3. Results

Unless otherwise stated, data is presented as means and standard deviations. The air-water fluxes and coincident supporting measurements are shown in Supplementary Material Table S1, and air-ice and air-snow fluxes are shown in Table S2. The uncertainties of the flux measurements shown in the Tables and Figures are the standard error of the samples within each

chamber deployment, and the uncertainties of the surface partial pressures in Table S1 and the Figures are the standard error of the samples comprising each measurement.

3.1 Meteorological and seawater conditions

Average wind speeds at 10 m, U_{10}, during SAS were 5.4 ± 2.4 m s^{-1} (Figs. 2b, 3a). The winds speeds corresponding to the air-water flux measurements were representative of the expedition as a whole with an average of 5.1 ± 2.7 m s^{-1}. Wind speeds were generally moderate, with ~ 80% of the U_{10} measurements between 2 and 6.5 m s-1 (Fig. 3a). The highest winds occurred early in the expedition, on August 8 and 9, with 20-minute average U_{10} reaching 13.4 m s^{-1}. The wind distribution is similar to that observed on previous summertime CAO measurement campaigns, though without the passage of frontal systems and the associated higher winds that occurred during some campaigns (e.g., Tjernström et al., 2012; Vüllers et al., 2021). Sea ice concentration was generally high, with 90% of the expedition occurring in SIC > 75%, and 60% of the expedition in SIC > 95% (Fig. 3b). The notable exception is a period from September 3 to September 7 when Oden was operating in a region of mixed sea ice and open water north of Greenland (Fig. 2c, Fig. 1).

Surface water temperature in leads sampled during flux measurements were -1.4 ± 0.5 °C (Fig. 4a), and the salinity of those samples showed high variation, ranging from 1.2 to 32.9, with an average 26.3 ± 8.5 (Fig. 4b). Surface water temperatures were generally at or very close to the seawater freezing point. Salinity lower than 22 occurred when ice movement caused a release of fresh meltpond water into leads, resulting in strong near-surface gradients. The temperature and salinity measured from the 8 m depth intake showed less variation, -1.2 ± 0.2 °C and 30.8 ± 1.2, respectively. Surface temperatures determined by infrared sensors, including both ice and water surfaces, were -2.0 ± 1.7 °C over the course of the expedition. Approximately 20% of the expedition occurred with surface temperatures below -3 °C, and 30% with surface temperatures above -1 °C (Fig. 3c).

Throughout the expedition, intermittent periods with falling surface temperatures occurred, associated with clear sky conditions and surface longwave cooling (e.g., Prytherch and Yelland, 2021). From August 25 there was a regime shift, with protracted periods of surface (ice) temperature below the seawater freezing point, and deeper intermittent surface temperature drops, falling to around -10 °C, indicating the beginning of the autumn freeze up (Supplementary Material Section 2 and Fig. S3).

3.2 CH_4 and CO_2 partial pressures

Atmospheric CH_4 partial pressure, pCH_4a, measured using the chamber LGR analyser during equilibration periods, increased from approximately 1.98 μatm to 2.01 μatm over the course of the expedition (mean and standard deviation 1.99 ± 0.02 μatm; Fig. 4c). The surface seawater pCH_4w was determined as the average of two GC-based sampling methods (Section 2.2), with the two methods having a mean standard error of 2.82 ± 1.54 μatm with the syringe-based samples consistently higher (Supplemental Materials Section 1; Figure S2a). The averaged surface seawater pCH_4w measurements were slightly

oversaturated throughout the expedition, 5.37 ± 3.13 μatm (Fig. 4c and Table S1). Overside samples were slightly higher and more variable (5.88 ± 4.32 μatm) than ice-based samples (5.05 ± 2.26 μatm), with the highest overside sample on August 29 at 16.0 μatm. The pCH_4w sampled from 8 m depth was lower and less variable than the surface measurements, with an average of 2.70 ± 0.68 μatm. The 8 m pCH_4w was closer to equilibrium than the surface waters, but still slightly oversaturated, most notably from August 18 to September 04 where pCH_4w averaged 3.1 ± 0.8 μatm.

Near surface gradients of CH_4 saturation determined from Ruttner bottle sampling and on-ship analysis during the latter part of the expedition showed little variation with depth over the upper 2.5 m (Fig. 5). A pronounced freshening of the near-surface water was observed on September 3 and 8, and to a lesser extent on August 27. This is likely to be either a residual layer from ice melt or due to leakage of fresh meltpond water resulting from ice movement caused by *Oden* 's nearby passing.

Atmospheric CO_2 partial pressure, pCO_2a, from chamber equilibration periods was 402.4 ± 3.0 μatm (Fig. 4d). The surface seawater pCO_2w was determined as the average of GC-based syringe samples and bottle samples analysed for DIC and TA from which pCO_2 was calculated (Section 2.2). The two methods had a mean standard error of 25.5 ± 22 μatm (Supplemental Materials Section 1; Figure S2b). The resulting averaged surface seawater pCO_2w was always undersaturated, with a mean value of 227 ± 71 μatm (Fig. 4d and Table S1). The pCO_2w from overside samples was higher and more variable (288 ± 69 μatm) than that from the ice-based samples (189 ± 39 μatm). The seawater pCO_2w from 8 m depth was closer to equilibrium but still strongly undersaturated during most of the expedition, on average 315 ± 28 μatm. There was a strong gradient in pCO_2w between the surface measurements and those from the 8 m intake from August 14 to the end of the expedition (Fig. 4d). Both depths were undersaturated throughout the expedition with the surface pCO_2w on average 88 μatm lower than at 8 m depth. The period prior to August 13 had noticeably higher surface water pCO_2w than later periods, close to or above the 8 m depth pCO_2w. The surface measurements in this early period were from both overside and ice-based sampling, suggesting this relatively reduced or reversed pCO_2w gradient was not primarily an artefact of *Oden's* influence on the upper water column.

3.3 Lead air-sea fluxes

All measured air-sea CH_4 fluxes were positive (emission from the water to the atmosphere), in the direction of the air-sea concentration gradient, and the majority of the fluxes were less than 5 μmol m^{-2} day^{-1} (Fig. 6a and Table S1). The two highest fluxes, on August 11 and August 29, were coincident with the strongest air-sea pCH_4 differences (Fig. 4c). The average air-sea CH_4 flux was 3.5 ± 4.4 μmol m^{-2} day^{-1}. The overside flux measurements were on average higher and more variable (6.7 ± 6.0 μmol m^{-2} day^{-1}) than the ice-based measurements (1.5 ± 1.1 μmol m^{-2} day^{-1}).

Measured air-sea CO_2 fluxes, using both the LGR- and Li-COR 7200-based systems, were all negative, showing uptake of CO_2 by seawater. The flux was in the direction of the air-sea concentration gradient, with a range of -1.5 to -20.7 mmol m^{-2} day^{-1} (Fig. 6a and Table S1). The average air-sea CO_2 flux was -7.3 ± 5.7 mmol m^{-2} day^{-1}. As for the CH_4 fluxes,

the average magnitude of the overside CO_2 flux measurements was higher and more variable (-12.7 ± 7.3 mmol m^{-2} day^{-1}) than the ice-based measurements (-4.8 ± 2.0 mmol m^{-2} day^{-1}).

The largest CO_2 fluxes occurred in the early part of the expedition, prior to August 13, during overside sampling and in a period with notably smaller air-sea pCO_2 gradient than later. The large overside flux measurements on August 8 occurred during high winds, but other high overside measurements on August 10 and 11 occurred during light winds < 4 m s^{-1} (Fig. 2b). These measurements may be biased by the presence of *Oden*, or the interaction between *Oden* and the floating chamber, affecting the near-surface turbulence that drives the flux. These biases likely depend on the interaction of conditions such as the wind speed and direction relative to *Oden*, the location and topology of sea ice, and the position of the chamber relative to *Oden* and to the sea ice, all of which varied from one sampling to another. As such, all overside flux measurements are treated separately to the ice-based measurements.

Thin, grease or frazil ice was present at times during the expedition, especially during the latter part of the expedition, from August 26, coinciding with the end of the melt season and the onset of the freeze up. Ice-based sampling when grease ice was present resulted in lower fluxes on average of CH_4 (0.9 ± 0.6 μmol m^{-2} day^{-1}), indicating that grease ice may impede gas exchange, presumably through the ice layer presenting both a physical barrier and reducing the action of wind on the surface water. However, the presence of grease ice did not change the average flux of CO_2, and the mean reduction of CH_4 flux is within the standard deviation. The presence of the chamber may modify the effect of the grease ice on gas exchange in an unquantified way, trapping ice inside or outside the chamber, and modifying the radiative balance at the surface, affecting ice formation.

3.4 Gas transfer velocities

Gas transfer velocities, k_{660}, determined directly from air-sea chamber flux measurements using Eqs. (1) and (2) were generally less than 10 cm hr^{-1}, with the notable exception of k_{660} determined from overside CO_2 flux measurements prior to August 13 when winds and fluxes were high (Fig. 6b). For all measurements, the average k_{660} was 6.7 ± 9.7 cm hr^{-1} (median 3.3 cm hr^{-1}). The average CH_4-flux derived k_{660} was 4.2 ± 4.6 cm hr^{-1} while the average CO_2-flux derived k_{660} was 8.0 ± 11.4 cm hr^{-1}. The distribution of k_{660} is non-Gaussian and the median values from both gases combined, and for CH_4 and CO_2 separately, are similar: 3.3, 3.8 and 3.1 cm hr^{-1} respectively. The ice-based measurements were lower and had less scatter, the median k_{660} of both gases was 2.5 cm hr^{-1} (average 3.0 ± 3.4 cm hr^{-1}). Many of the lower k_{660} measurements were made in the presence of grease or frazil ice, with the median k_{660} of grease-ice affected, ice-based samples of both gases being 1.1 cm hr^{-1} (average 1.4 ± 0.9 cm hr^{-1}).

The wind speed dependence of the measurements, determined with non-linear least squares fit of the form $y = a \times x^b$, was approximately cubic, though the correlation with the data was weak (a = 0.02, b = 2.9, r^2 = 0.31; Fig. 7). The two measurements with greatest uncertainty (standard errors of 289 and 45 cm hr^{-1}) were excluded from the fit. The relatively few data points (36) and the weakness of the correlation means that caution is needed in interpretation or application of this relationship. At low wind speeds (< 3 m s^{-1}), the measurements are higher than previously determined power law

parameterisations, suggesting that processes other than wind speed may be contributing to interfacial mixing. With the exception of one value, these low wind k_{660} are relatively small, similar to the low-wind values of previous parameterisations determined with non-zero intercepts (e.g., Wanninkhof et al., 2009).

The overside CO_2 flux derived k_{660} were higher and more scattered than the other measurements and may have been affected by their close proximity to *Oden's* hull and the additional turbulence that this may induce in the ocean. The wind speed dependence of the fit determined to only ice-based measurements (again excluding the measurement with highest standard error) was weaker and had a weaker correlation ($a = 0.999$, $b = 0.533$, $r^2 = 0.13$). The ice-based measurements would not have been affected by any such bias, and the wind speed dependence of ice-based CO_2- and CH_4-derived k_{660} was weaker, close to linear, and generally below previous open ocean and lead water k_{660} parameterisations. The contribution to the observed k_{660} wind speed dependence of forcings particular to the sea-ice environment are discussed in Section 4.2.

The measurements were also compared with the parametric Wave Age Gas Transfer (WAGT) model of gas exchange in sea ice regions (Bigdeli et al., 2018). The WAGT model was run in both SIC mode, with SIC set to 90%, and in fetch mode using the lead width measurements. The WAGT fetch mode has good agreement with the measurements at wind speeds below 6 m s^{-1} whereas the SIC mode overpredicts. Both WAGT modes over predict at higher wind speeds.

3.5 Air-snow fluxes

Chamber measurements of air-snow CO_2 flux showed consistent small fluxes, on average, -1.1 ± 1.2 mmol m^{-2} day^{-1}, with the largest magnitude flux -2.9 mmol m^{-2} day^{-1} (Fig. 6c and Table S2). No clear dependence of the atmospheric flux on surface temperature was found, with the largest magnitude fluxes occurring at temperatures close to and above freezing, but some relatively large fluxes (up to -2.8 mmol m^{-2} day^{-1}) also being observed during the coldest measured surface conditions, with temperatures < -2°C (Fig. 8).

4. Discussion

4.1 Near-surface concentration gradients

Strong near-surface CO_2 gradients are often observed in Arctic waters. Lower CO_2 partial pressure at the surface relative to 8 m (Fig. 4d) may result from the input of unsaturated water from melting sea ice, from differences in biological activity, and from the increased solubility resulting from the generally lower temperature and fresher surface waters (Figs. 4a, b). Solubility differences between the surface and 8 m in the measurements reported here on average account for a pCO_2w difference of 10 μatm, or 11% of the total average difference between the depths. The fresher surface layer observed on several days (August 27, September 3 and 8; Fig. 5) indicates a stratification that could act to suppress near-surface mixing, leading to lower surface gas concentrations and thus lower fluxes. In the coarse vertical resolution observations reported here, near-surface CH_4

saturations decrease in the presence of lower salinity, suggesting that in these cases the greater solubility in fresher water compensates for any stratification effect.

The results here further demonstrate the concentration gradients that can be present between the surface and the sampling depths used for the majority of the reported ocean 'surface' gas concentration measurement (e.g., Miller et al., 2019). Larger air-sea concentration differences will, all else being equal, cause a larger air-sea flux, and thus any gradient between the surface and the water sampling depth will bias both bulk-method fluxes (i.e., fluxes calculated using Eq. (1) and a parameterisation of k; Wanninkhof et al., 2009) and gas transfer velocity measurements. As such gradients are common, and are not easy to determine or correct for, many parameterisations of gas transfer incorporate such biases.

If the surface partial pressure, T and S measurements from this study are used to determine bulk-method fluxes, the CO_2 fluxes are on average 77% (with the k-U_{10} relationship of Ho et al., 2006) or 25% (with the k-U_{10} relationship of Prytherch and Yelland, 2021) higher than the measured chamber fluxes (Table 1). This result adds to the existing literature showing a physical effect of sea ice on gas transfer velocity. In contrast, if the 8 m depth partial pressure, T and S measurements are used instead, the bulk fluxes are 1% (Ho et al., 2006) and 30% lower (Prytherch and Yelland, 2021) than the measured fluxes. This result adds to those discussing the bias in bulk fluxes, particularly prevalent in the Arctic, when gas concentration measurements are made at depth below the air-water interface (e.g. Miller et al., 2019). For CH_4 the effects of the gradients are similar (Table 1), with bulk fluxes derived from surface measurements being larger than the chamber fluxes by 156% and 80% (for the Ho et al., 2006, and Prytherch and Yelland, 2021 k-U_{10} relationships, respectively) and the bulk fluxes derived from 8 m measurements being smaller than the chamber flux measurements by 28% and 49% respectively.

4.2 Gas transfer in the presence of sea ice

Greater lead width and fetch enables greater wind-driven mixing, while measurements close to ice edges may also be affected by the interaction of wind and waves with the ice edge. The wind speed dependence of all (36) measurements (Fig. 7) is approximately cubic with a weak correlation (r^2 0.31). The k_{660} measurements, normalised by U_{10}, do not show a clear dependence on lead width as determined by laser ranging (Fig. 9). For overside measurements lead width was the distance from *Oden's* hull to the ice edge. In contrast, the U_{10}-normalised ice-based measurements appear to have a dependence on lead width; the correlation of a non-linear least squares fit of the form $y = a \times x^b$ is weak (a = 0.208, b = 0.34, r^2 = 0.27) but stronger than the fit of these measurements to wind speed. Properly accounting for such fetch effects would require determination of lead dimensions, relative wind direction and ice freeboard, but the relatively small variation of the ice-based measurements with width suggests that simpler approaches to parameterising k in sea-ice regions, with either a wind speed dependence or a constant value, may be sufficient.

The buoyancy flux measurements enable Identification of measurements made in conditions of surface cooling-induced convection, which can enhance gas exchange (McGillis et al., 2004), but no clear enhancement of gas transfer was apparent (Fig. 7). Many of the convective measurements were also in leads of < 10 m width (Figs. 7, 9) complicating determination of the impact of either convection or fetch on gas exchange. Many, but not all, of the lower gas exchange rates

were measured when grease ice was present on the lead water, even at higher wind speeds (> 7 m s^{-1}) when low lead widths provided sheltered conditions (Fig. 7). Grease ice is expected to reduce gas transfer rates, and all high k_{660} measurements (> 5 cm hr^{-1}), both overside and ice-based, were obtained when grease ice was not present.

The WAGT) model was designed to use estimates of the area of open water from SIC products. Although different ice products have experienced significant improvements in increased resolution in recent years, they are still prone to missing critical small-scale features such as open or refrozen leads. Passive radiometer data also treats a ~20 cm thin ice cover as open water (e.g. Hoffman et al., 2019), with severe impacts on gas transfer estimates.

4.3 Regional fluxes

The fluxes and gas transfer measurements presented here provide direct measurement-based constraints for the role of the CAO in CO_2 and CH_4 atmospheric exchange. Air-sea chamber fluxes were made at latitudes from approximately 82.5°N to 90°N. These latitudes bound an area of 2.2 x 10^6 km^2, approximately corresponding to the deep-water areas of the Amundsen basin. The IHO-defined central Arctic deep basin (4.7 x 10^6 km^2), and the bathymetrically-defined 4.5 x 10^6 km^2 "Central Arctic Ocean Basin" delineated by Jakobsson (2002) and used here as the definition of the CAO are larger. In all definitions, the CAO corresponds to the Arctic Ocean deep water > 2400 m depth, as a strong contrast to the shallow shelf seas (average depths ~50-250 m) which surround the Arctic Ocean. The average SIC during this portion of the expedition was 90%, determined from AMSR-2 6.25km^2 observations using the ASI algorithm (Spreen et al., 2008).

The measured air-sea CO_2 fluxes are of similar magnitude to the EC measurements of Prytherch et al. (2017) (average -7.8 mmol m^{-2} day^{-1}), Prytherch and Yelland (2021) (0 to -20 mmol m^{-2} day^{-1}, average -12.4 mmol m^{-2} day^{-1}, measured in higher winds), and of Dong et al. (2021), (0 to -40 mmol m^{-2} day^{-1}, measured in SIC > 60%). Averaging observations regionally, the mean chamber-derived CO_2 air-sea fluxes of -7.6 mmol m^{-2} day^{-1} correspond to SIC-accounted CAO fluxes of -3.42 x10^9 mol day^{-1}, or -150.5 Gg CO_2 day^{-1}. The flux measurements reported here were made during the summer and the beginning of the autumn freeze up in conditions of persistent, strong pCO_2w undersaturation. The annual cycle of Arctic Ocean surface pCO_2w is poorly constrained, primarily due to the rarity of reported observations outside of summer months (e.g. Yasunaka et al., 2018; Else et al., 2012). As such, while we can estimate an annual CAO air-sea flux of -55.0 Tg CO_2 yr^{-1} by multiplying the average daily flux by 365. this result is highly uncertain. Furthermore, while density stratification from sea-ice melt in summer months may suppress upper ocean mixing leading to reduced air-sea concentration gradients and thus reduced summer fluxes relative to other seasons, this stratification was not evident in the measurements reported here. Thus, due to the higher SIC and lower primary productivity in winter months, our annual flux estimate is likely to represent a high estimate. If the average bulk flux of -8.4 mmol m^{-2} day^{-1} as determined from near-surface CO_2 concentrations and the k relationship of Prytherch and Yelland (2021) is used instead of the average observed flux, the CAO air-sea flux is slightly larger, -3.78 x10^9 mol day^{-1}, or -166.4 Gg CO_2 day^{-1}.

The measured air-snow CO_2 fluxes (-1.1 ± 1.2 mmol m^{-2} day^{-1}) are a similar magnitude to previously reported EC-determined air-snow fluxes from the summertime CAO (Prytherch and Yelland, 2021; -0.7 mmol m^{-2} day^{-1}, maximum -6.5

mmol m^{-2} day^{-1}). They also span a similar range (-2.9 to 0.25 mmol m^{-2} day^{-1}) including the observed positive emission fluxes, as previously reported air-snow chamber flux measurements (Geilfus et al., 2012, Nomura et al., 2010, 2013, 2018, Delille et al., 2014, Geiflus et al., 2015). However, none of these previously reported air-snow flux measurements are from the summertime or autumn CAO. Using the observed expedition SIC and the average flux through snow-covered sea ice of -1.1 mmol m^{-2} day^{-1} yields a CAO regional air-snow flux of -4.46 x 10^9 mol day^{-1}, or -196.1 Gg day^{-1}. Combining the air-sea and air-snow chamber flux estimates with constant SIC (90%), the average atmospheric CO_2 flux for the CAO is -1.75 mmol m^{-2} day^{-1}.

The average air-sea CH_4 flux of 3.5 μmol m^{-2} day^{-1}, accounting for SIC, equates to a CAO flux of 1.58 x 10^6 mol day^{-1}, or 25.3 Mg day^{-1}. Similarly, the average bulk CH_4 flux of 5 μmol m^{-2} day^{-1} derived from near-surface CH_4 concentrations and the *k* relationship of Prytherch and Yelland (2021) corresponds to 36.1 Mg day^{-1} for the CAO area. The annual cycle of Arctic Ocean surface CH_4 is much less well known than for CO_2, in particular the origin of the dissolved CH_4 driving the observed fluxes. As such the extrapolation of our observations and bulk estimates to annual fluxes (9.2 Gg yr^{-1} and 13.2 Gg yr^{-1} respectively) is also highly uncertain. Both the directly observed and bulk flux-derived annual estimates are likely to be high estimates due to the higher SIC and minimal release of CH_4 from within sea ice during winter.

Stratification of near surface waters by freshening from melt water may reduce air-sea gas flux by both reducing the turbulent mixing below the interfacial layer, dampening the gas transfer velocity, and by impeding the replenishment of the equilibrating surface waters from the bulk water below, reducing the concentration difference that drives the exchange. Suppression of turbulent mixing may contribute to the observed difference between chamber and bulk fluxes, however, the surface layer freshwater stratification apparent in surface layers did not coincide with CH_4 stratification (Fig. 5).

Both the direct chamber CH_4 fluxes and bulk CH_4 fluxes are of similar magnitude to previously reported flux estimates derived from seawater CH_4 measurements in summer and winter at more southerly Arctic marine locations (e.g. Lorenson et al., 2016; Manning et al., 2020, 2022; Fenwick et al., 2017; Silyakova et al., 2022), but are approximately 35 times smaller than aircraft-based observations of fluxes from wintertime leads over the western CAO's Canada Basin, south of 82 N (Kort et al., 2012). This suggests a strong seasonal dependence in CAO CH_4 flux, or that the aircraft-based measurements of large fluxes represent episodic rather than typical widespread emissions, or erroneous measurements. If we assume that the fluxes reported by Kort et al. are more typical of the Canada Basin and distinct from our primarily Amundsen basin study area, this suggests a much higher net annual CH_4 flux from the CAO of up to ~0.1 Tg yr^{-1}. The CAO has a mean depth > 2700 m (Jakobsson, 2002), meaning any CH_4 emissions must be from near-surface production or long-range transport of dissolved CH_4; seafloor sources are too deep to significantly affect the surface pCH_4w in the CAO.

5. Conclusions

The direct flux and gas transfer measurements presented in this study offer insights into the role of the CAO in atmospheric exchange of climate forcing trace gases, informing future climate modelling and carbon budget analysis. They provide a

measurement-based constraint on the magnitude of the CAO CO_2 flux, with the observed CAO CO_2 flux in agreement with the observation-based estimates of Bates et al. (2006) and Yasunaka et al., (2018), and an order of magnitude greater than the coupled ocean-biogeochemistry model estimate of Manizza et al., 2019. For CH_4, the direct measurement-based constraints determined here show that the CAO is a very small additional contributor to the Arctic Ocean CH_4 flux in summer, with the mean CAO CH_4 flux of 25.3 Mg day^{-1} comprising approximately $1/500^{th}$ of the estimate of integrated Arctic marine CH_4 emissions of 4-5 Tg yr^{-1} (Thornton et al, 2016a; 2016b; 2020) if that estimate is assumed evenly distributed over the year. Arctic marine CH_4 emissions are dominated by the shallow coastal shelf emissions.

While the observed gas transfer velocities had a similar, if weakly correlated, wind-speed dependence to that of Prytherch and Yelland (2021), the wind-speed dependence of the ice-based measurements, free from any influence of *Oden* on the exchange rate, was much weaker. The measurements reported here, from pack ice regions with small water surfaces, could be appropriately represented with a constant k_{660}, 2.5 cm hr^{-1} instead of a relationship directly or indirectly (i.e. wave or turbulence-based) dependent on wind speed. In areas such as the marginal ice zone with mixed sea ice and water and larger fetches, the direct and indirect influence of wind on interfacial mixing will be greater and gas exchange should be represented using a parameterisation incorporating wind-speed such as Prytherch and Yelland (2021).

Author contributions

JP designed the experiment, JP and SM carried out the flux measurements and water sampling, JP, IB, VB, AU, AH, AN and LH analysed the water samples. JP, BT and MT developed the ship-based instrumentation, and JP and VB developed the chamber flux systems. JP prepared the manuscript with contributions from all co-authors.

Acknowledgements

The Swedish Polar Research Secretariat (SPRS) provided access to the icebreaker (I/B) Oden and logistical support. We would like to thank Capt. Mattias Petersson and the crew of *Oden* for their invaluable support throughout the field campaign. Thanks also to the Chief Scientist Pauline Snoeijs Leijonmalm for the planning and coordination of SAS2021.

Financial support

JP and SM were supported by the Knut and Alice Wallenberg Foundation (grant no. 2016-0024). AU was supported by the Swedish Research Council Formas (grant no. 2018-01398) and the Hasselblad Foundation (grant no. 2019-1218). LAH was supported by the Arctic Research Icebreaker Consortium (ARICE, EU, https://arice-h2020.eu) (grant no. 730 965). This paper contributes to the science plan of the Surface Ocean-Lower Atmosphere Study (SOLAS), which is partially supported by the U.S. National Science Foundation (Grant OCE-1840868) via the Scientific Committee on Oceanic Research (SCOR).

References

Ahmed, M. M. M., Else, B. G. T., Capelle, D., Miller, L. A., and Papakyriakou, T.: Underestimation of surface pCO2 and air-sea CO2 fluxes due to freshwater stratification in an Arctic shelf sea, Hudson Bay, Elementa: Science of the Anthropocene, 8, https://doi.org/10.1525/elementa.084, 2020.

Bastviken, D., Ejlertsson, J., Sundh, I., and Tranvik, L.: METHANE AS A SOURCE OF CARBON AND ENERGY FOR LAKE PELAGIC FOOD WEBS, Ecology, 84, 969–981, https://doi.org/10.1890/0012-9658(2003)084[0969:maasoc]2.0.co;2, 2003.

Bates, N. R. and Mathis, J. T.: The Arctic Ocean marine carbon cycle: evaluation of air-sea CO2 exchanges, ocean acidification impacts and potential feedbacks, Biogeosciences, 6, 2433–2459, https://doi.org/10.5194/bg-6-2433-2009, 2009.

Bates, N. R., Moran, S. B., Hansell, D. A., and Mathis, J. T.: An increasing CO2 sink in the Arctic Ocean due to sea-ice loss, Geophys. Res. Lett., 33, https://doi.org/10.1029/2006gl027028, 2006.

Bigdeli, A., Hara, T., Loose, B., and Nguyen, A. T.: Wave Attenuation and Gas Exchange Velocity in Marginal Sea Ice Zone, J. Geophys. Res. Oceans, 123, 2293–2304, https://doi.org/10.1002/2017jc013380, 2018.

Butterworth, B. J. and Miller, S. D.: Air-sea exchange of carbon dioxide in the Southern Ocean and Antarctic marginal ice zone, Geophys. Res. Lett., 43, 7223–7230, https://doi.org/10.1002/2016gl069581, 2016.

Cole, J. J., Bade, D. L., Bastviken, D., Pace, M. L., and Van de Bogert, M.: Multiple approaches to estimating air-water gas exchange in small lakes, Limnol. Oceanogr. Methods, 8, 285–293, https://doi.org/10.4319/lom.2010.8.285, 2010.

Damm, E., Rudels, B., Schauer, U., Mau, S., and Dieckmann, G.: Methane excess in Arctic surface water- triggered by sea ice formation and melting, Sci Rep, 5, https://doi.org/10.1038/srep16179, 2015.

Damm, E., Bauch, D., Krumpen, T., Rabe, B., Korhonen, M., Vinogradova, E., and Uhlig, C.: The Transpolar Drift conveys methane from the Siberian Shelf to the central Arctic Ocean, Sci Rep, 8, https://doi.org/10.1038/s41598-018-22801-z, 2018.

Delille, B., Vancoppenolle, M., Geilfus, N.-X., Tilbrook, B., Lannuzel, D., Schoemann, V., Becquevort, S., Carnat, G., Delille, D., Lancelot, C., Chou, L., Dieckmann, G. S., and Tison, J.-L.: Southern Ocean CO2 sink: The contribution of the sea ice, J. Geophys. Res. Oceans, 119, 6340–6355, https://doi.org/10.1002/2014jc009941, 2014.

Dickson, A.G., Sabine, C.L. and Christian, J.R. (Eds.). Guide to Best Practices for Ocean CO_2 Measurements. PICES Special Publication 3, 191 pp. 2007.

Dong, Y., Yang, M., Bakker, D. C. E., Liss, P. S., Kitidis, V., Brown, I., Chierici, M., Fransson, A., and Bell, T. G.: Near-Surface Stratification Due to Ice Melt Biases Arctic Air-Sea CO2 Flux Estimates, Geophysical Research Letters, 48, https://doi.org/10.1029/2021gl095266, 2021.

Else, B. G. T., Papakyriakou, T. N., Galley, R. J., Mucci, A., Gosselin, M., Miller, L. A., Shadwick, E. H., and Thomas, H.: Annual cycles of pCO2sw in the southeastern Beaufort Sea: New understandings of air-sea CO2 exchange in arctic polynya regions, J. Geophys. Res., 117, https://doi.org/10.1029/2011jc007346, 2012.

Fairall, C. W., Yang, M., Brumer, S. E., Blomquist, B. W., Edson, J. B., Zappa, C. J., Bariteau, L., Pezoa, S., Bell, T. G., and Saltzman, E. S.: Air-Sea Trace Gas Fluxes: Direct and Indirect Measurements, Front. Mar. Sci., 9, https://doi.org/10.3389/fmars.2022.826606, 2022.

Fanning, K. A. and Torres, L. M.: 222Rn and226Ra: indicators of sea-ice effects on air-sea gas exchange, Polar Research, 10, 51–58, https://doi.org/10.3402/polar.v10i1.6727, 1991.

Fenwick, L., Capelle, D., Damm, E., Zimmermann, S., Williams, W. J., Vagle, S., and Tortell, P. D.: Methane and nitrous oxide distributions across the North American Arctic Ocean during summer, 2015, J. Geophys. Res. Oceans, 122, 390–412, https://doi.org/10.1002/2016jc012493, 2017.

Fransson, A., Chierici, M., Skjelvan, I., Olsen, A., Assmy, P., Peterson, A. K., Spreen, G., and Ward, B.: Effects of sea-ice and biogeochemical processes and storms on under-ice water f CO2 during the winter-spring transition in the high AO: Implications for sea-air CO2 fluxes, J. Geophys. Res. Oceans, 122, 5566–5587, https://doi.org/10.1002/2016jc012478, 2017.

Geilfus, N.-X., Carnat, G., Papakyriakou, T., Tison, J.-L., Else, B., Thomas, H., Shadwick, E., and Delille, B.: Dynamics of pCO2 and related air-ice CO2 fluxes in the Arctic coastal zone (Amundsen Gulf, Beaufort Sea), J. Geophys. Res., 117, n/a-n/a, https://doi.org/10.1029/2011jc007118, 2012.

Geilfus, N.-X., Galley, R. J., Crabeck, O., Papakyriakou, T., Landy, J., Tison, J.-L., and Rysgaard, S.: Inorganic carbon dynamics of melt-pond-covered first-year sea ice in the Canadian Arctic, Biogeosciences, 12, 2047–2061, https://doi.org/10.5194/bg-12-2047-2015, 2015.

Gålfalk, M., Bastviken, D., Fredriksson, S., and Arneborg, L.: Determination of the piston velocity for water-air interfaces using flux chambers, acoustic Doppler velocimetry, and IR imaging of the water surface, J. Geophys. Res. Biogeosci., 118, 770–782, https://doi.org/10.1002/jgrg.20064, 2013.

Haraldsson, C., Anderson, L. G., Hassellöv, M., Hulth, S., and Olsson, K.: Rapid, high-precision potentiometric titration of alkalinity in ocean and sediment pore waters, Deep Sea Research Part I: Oceanographic Research Papers, 44, 2031–2044, https://doi.org/10.1016/s0967-0637(97)00088-5, 1997.

Ho, D. T., Law, C. S., Smith, M. J., Schlosser, P., Harvey, M., and Hill, P.: Measurements of air-sea gas exchange at high wind speeds in the Southern Ocean: Implications for global parameterizations, Geophys. Res. Lett., 33, https://doi.org/10.1029/2006gl026817, 2006.

Hoffman, J., Ackerman, S., Liu, Y., and Key, J.: The Detection and Characterization of Arctic Sea Ice Leads with Satellite Imagers, Remote Sensing, 11, 521, https://doi.org/10.3390/rs11050521, 2019.

Van Heuven, S., Pierrot, D., Rae, J. W. B., Lewis, E., and Wallace, D. W. R.: MATLAB Program Developed for CO2 System Calculations. ORNL/CDIAC-105b., https://doi.org/10.3334/CDIAC/OTG.CO2SYS_MATLAB_V1.1, 2011.

Jähne, B., Münnich, K. O., Bösinger, R., Dutzi, A., Huber, W., and Libner, P.: On the parameters influencing air-water gas exchange, J. Geophys. Res., 92, 1937, https://doi.org/10.1029/jc092ic02p01937, 1987.

Jakobsson, M.: Hypsometry and volume of the Arctic Ocean and its constituent seas, Geochem.-Geophys.-Geosyst., 3, 1–18, https://doi.org/10.1029/2001gc000302, 2002.

Johnson, K. M., Sieburth, J. M., Williams, P. J. leB, and Brändström, L.: Coulometric total carbon dioxide analysis for marine studies: Automation and calibration, Marine Chemistry, 21, 117–133, https://doi.org/10.1016/0304-4203(87)90033-8, 1987.

Kort, E. A., Wofsy, S. C., Daube, B. C., Diao, M., Elkins, J. W., Gao, R. S., Hintsa, E. J., Hurst, D. F., Jimenez, R., Moore, F. L., Spackman, J. R., and Zondlo, M. A.: Atmospheric observations of Arctic Ocean methane emissions up to 82° north, Nature Geosci, 5, 318–321, https://doi.org/10.1038/ngeo1452, 2012.

Kwok, R.: Arctic sea ice thickness, volume, and multiyear ice coverage: losses and coupled variability (1958–2018), Environ. Res. Lett., 13, 105005, https://doi.org/10.1088/1748-9326/aae3ec, 2018.

Lewis, E., and D. W. R. Wallace. Program Developed for CO2 System Calculations. ORNL/CDIAC-105. Carbon Dioxide Information Analysis Center, Oak Ridge National Laboratory, U.S. Department of Energy, Oak Ridge, Tennessee. 1988.

Loose, B., Schlosser, P., Perovich, D., Ringelberg, D., Ho, D. T., Takahashi, T., Richter-Menge, J., Reynolds, C. M., Mcgillis, W. R., and Tison, J.-L.: Gas diffusion through columnar laboratory sea ice: implications for mixed-layer ventilation of CO2 in the seasonal ice zone, Tellus B: Chemical and Physical Meteorology, 63, 23, https://doi.org/10.1111/j.1600-0889.2010.00506.x, 2011.

Loose, B., McGillis, W. R., Perovich, D., Zappa, C. J., and Schlosser, P.: A parameter model of gas exchange for the seasonal sea ice zone, Ocean Sci., 10, 17–28, https://doi.org/10.5194/os-10-17-2014, 2014.

Loose, B., Kelly, R. P., Bigdeli, A., Williams, W., Krishfield, R., Rutgers van der Loeff, M., and Moran, S. B.: How well does wind speed predict air-sea gas transfer in the sea ice zone? A synthesis of radon deficit profiles in the upper water column of Arctic Ocean, JGR Oceans, 122, 3696–3714, https://doi.org/10.1002/2016jc012460, 2017.

Lovely, A., Loose, B., Schlosser, P., McGillis, W., Zappa, C., Perovich, D., Brown, S., Morell, T., Hsueh, D., and Friedrich, R.: The Gas Transfer through Polar Sea ice experiment: Insights into the rates and pathways that determine geochemical fluxes, J. Geophys. Res. Oceans, 120, 8177–8194, https://doi.org/10.1002/2014jc010607, 2015.

Lorenson, T. D., Greinert, J., and Coffin, R. B.: Dissolved methane in the Beaufort Sea and the Arctic Ocean, 1992-2009; sources and atmospheric flux, Limnol. Oceanogr., 61, S300–S323, https://doi.org/10.1002/lno.10457, 2016.

Lorke, A., Bodmer, P., Noss, C., Alshboul, Z., Koschorreck, M., Somlai-Haase, C., Bastviken, D., Flury, S., McGinnis, D. F., Maeck, A., Müller, D., and Premke, K.: Technical note: drifting versus anchored flux chambers for measuring greenhouse gas emissions from running waters, Biogeosciences, 12, 7013–7024, https://doi.org/10.5194/bg-12-7013-2015, 2015.

Lueker, T. J., Dickson, A. G., and Keeling, C. D.: Ocean pCO2 calculated from dissolved inorganic carbon, alkalinity, and equations for K1 and K2: validation based on laboratory measurements of CO2 in gas and seawater at equilibrium, Marine Chemistry, 70, 105–119, https://doi.org/10.1016/s0304-4203(00)00022-0, 2000.

MacIntyre, S., Fram, J. P., Kushner, P. J., Bettez, N. D., O'Brien, W. J., Hobbie, J. E., and Kling, G. W.: Climate-related variations in mixing dynamics in an Alaskan arctic lake, Limnol. Oceanogr., 54, 2401–2417, https://doi.org/10.4319/lo.2009.54.6_part_2.2401, 2009.

MacIntyre, S., Jonsson, A., Jansson, M., Aberg, J., Turney, D. E., and Miller, S. D.: Buoyancy flux, turbulence, and the gas transfer coefficient in a stratified lake, Geophys. Res. Lett., 37, n/a-n/a, https://doi.org/10.1029/2010gl044164, 2010.

Manizza, M., Menemenlis, D., Zhang, H., and Miller, C. E.: Modeling the Recent Changes in the Arctic Ocean CO2 Sink (2006–2013), Global Biogeochem. Cycles, 33, 420–438, https://doi.org/10.1029/2018gb006070, 2019.

Mannich, M., Fernandes, C. V. S., and Bleninger, T. B.: Uncertainty analysis of gas flux measurements at air–water interface using floating chambers, Ecohydrology & Hydrobiology, 19, 475–486, https://doi.org/10.1016/j.ecohyd.2017.09.002, 2019.

Manning, C. C. M., Zheng, Z., Fenwick, L., McCulloch, R. D., Damm, E., Izett, R. W., Williams, W. J., Zimmermann, S., Vagle, S., and Tortell, P. D.: Interannual Variability in Methane and Nitrous Oxide Concentrations and Sea-Air Fluxes Across the North American Arctic Ocean (2015–2019), Global Biogeochemical Cycles, 36, https://doi.org/10.1029/2021gb007185, 2022.

Manning, C. C., Preston, V. L., Jones, S. F., Michel, A. P. M., Nicholson, D. P., Duke, P. J., Ahmed, M. M. M., Manganini, K., Else, B. G. T., and Tortell, P. D.: River Inflow Dominates Methane Emissions in an Arctic Coastal System, Geophys. Res. Lett., 47, https://doi.org/10.1029/2020gl087669, 2020.

Matthews, C. J. D., St.Louis, V. L., and Hesslein, R. H.: Comparison of Three Techniques Used To Measure Diffusive Gas Exchange from Sheltered Aquatic Surfaces, Environ. Sci. Technol., 37, 772–780, https://doi.org/10.1021/es0205838, 2003.

Marcq, S. and Weiss, J.: Influence of sea ice lead-width distribution on turbulent heat transfer between the ocean and the atmosphere, The Cryosphere, 6, 143–156, https://doi.org/10.5194/tc-6-143-2012, 2012.

McGillis, W. R. and Wanninkhof, R.: Aqueous CO2 gradients for air–sea flux estimates, Marine Chemistry, 98, 100–108, https://doi.org/10.1016/j.marchem.2005.09.003, 2006.

Miller, L. A., Fripiat, F., Else, B. G. T., Bowman, J. S., Brown, K. A., Collins, R. E., Ewert, M., Fransson, A., Gosselin, M., Lannuzel, D., Meiners, K. M., Michel, C., Nishioka, J., Nomura, D., Papadimitriou, S., Russell, L. M., Sørensen, L. L., Thomas, D. N., Tison, J.-L., van Leeuwe, M. A., Vancoppenolle, M., Wolff, E. W., and Zhou, J.: Methods for biogeochemical studies of sea ice: The state of the art, caveats, and recommendations, edited by: Deming, J. W. and Ackley, S. F., Elementa: Science of the Anthropocene, 3, https://doi.org/10.12952/journal.elementa.000038, 2015.

Miller, L. A., Burgers, T. M., Burt, W. J., Granskog, M. A., and Papakyriakou, T. N.: Air-Sea CO2 Flux Estimates in Stratified Arctic Coastal Waters: How Wrong Can We Be?, Geophys. Res. Lett., 46, 235–243, https://doi.org/10.1029/2018gl080099, 2019.

Mortin, J., Graversen, R. G., and Svensson, G.: Evaluation of pan-Arctic melt-freeze onset in CMIP5 climate models and reanalyses using surface observations, Clim Dyn, 42, 2239–2257, https://doi.org/10.1007/s00382-013-1811-z, 2013.

Nomura, D., Yoshikawa-Inoue, H., Toyota, T., and Shirasawa, K.: Effects of snow, snowmelting and refreezing processes on air–sea-ice CO2 flux, J. Glaciol., 56, 262–270, https://doi.org/10.3189/002214310791968548, 2010.

Nomura, D., Granskog, M. A., Assmy, P., Simizu, D., and Hashida, G.: Arctic and Antarctic sea ice acts as a sink for atmospheric CO2 during periods of snowmelt and surface flooding, J. Geophys. Res. Oceans, 118, 6511–6524, https://doi.org/10.1002/2013jc009048, 2013.

Nomura, D., Granskog, M. A., Fransson, A., Chierici, M., Silyakova, A., Ohshima, K. I., Cohen, L., Delille, B., Hudson, S. R., and Dieckmann, G. S.: CO2 flux over young and snow-covered Arctic pack ice in winter and spring, Biogeosciences, 15, 3331–3343, https://doi.org/10.5194/bg-15-3331-2018, 2018.

Onarheim, I. H., Eldevik, T., Smedsrud, L. H., and Stroeve, J. C.: Seasonal and Regional Manifestation of Arctic Sea Ice Loss, J. Climate, 31, 4917–4932, https://doi.org/10.1175/jcli-d-17-0427.1, 2018.

Ouyang, Z., Li, Y., Qi, D., Zhong, W., Murata, A., Nishino, S., Wu, Y., Jin, M., Kirchman, D., Chen, L., and Cai, W.: The Changing CO2 Sink in the Western Arctic Ocean From 1994 to 2019, Global Biogeochemical Cycles, 36, https://doi.org/10.1029/2021gb007032, 2022.

Parmentier, F.-J. W., Christensen, T. R., Sørensen, L. L., Rysgaard, S., McGuire, A. D., Miller, P. A., and Walker, D. A.: The impact of lower sea-ice extent on Arctic greenhouse-gas exchange, Nature Clim Change, 3, 195–202, https://doi.org/10.1038/nclimate1784, 2013.

Prytherch, J. and Yelland, M. J.: Wind, Convection and Fetch Dependence of Gas Transfer Velocity in an Arctic Sea-Ice Lead Determined From Eddy Covariance CO2 Flux Measurements, Global Biogeochem Cycles, 35, https://doi.org/10.1029/2020gb006633, 2021.

Prytherch, J., Brooks, I. M., Crill, P. M., Thornton, B. F., Salisbury, D. J., Tjernström, M., Anderson, L. G., Geibel, M. C., and Humborg, C.: Direct determination of the air-sea CO2 gas transfer velocity in Arctic sea ice regions, Geophys. Res. Lett., 44, 3770–3778, https://doi.org/10.1002/2017gl073593, 2017.

Rantanen, M., Karpechko, A. Yu., Lipponen, A., Nordling, K., Hyvärinen, O., Ruosteenoja, K., Vihma, T., and Laaksonen, A.: The Arctic has warmed nearly four times faster than the globe since 1979, Commun Earth Environ, 3, https://doi.org/10.1038/s43247-022-00498-3, 2022.

Rigor, I. G., Colony, R. L., and Martin, S.: Variations in Surface Air Temperature Observations in the Arctic, 1979–97, J. Climate, 13, 896–914, https://doi.org/10.1175/1520-0442(2000)013<0896:visato>2.0.co;2, 2000.

Rutgers van der Loeff, M. M., Cassar, N., Nicolaus, M., Rabe, B., and Stimac, I.: The influence of sea ice cover on air-sea gas exchange estimated with radon-222 profiles, J. Geophys. Res. Oceans, 119, 2735–2751, https://doi.org/10.1002/2013jc009321, 2014.

Saunois, M., Stavert, A. R., Poulter, B., Bousquet, P., Canadell, J. G., Jackson, R. B., Raymond, P. A., Dlugokencky, E. J., Houweling, S., Patra, P. K., Ciais, P., Arora, V. K., Bastviken, D., Bergamaschi, P., Blake, D. R., Brailsford, G., Bruhwiler, L., Carlson, K. M., Carrol, M., Castaldi, S., Chandra, N., Crevoisier, C., Crill, P. M., Covey, K., Curry, C. L., Etiope, G., Frankenberg, C., Gedney, N., Hegglin, M. I., Höglund-Isaksson, L., Hugelius, G., Ishizawa, M., Ito, A., Janssens-Maenhout, G., Jensen, K. M., Joos, F., Kleinen, T., Krummel, P. B., Langenfelds, R. L., Laruelle, G. G., Liu, L., Machida, T., Maksyutov, S., McDonald, K. C., McNorton, J., Miller, P. A., Melton, J. R., Morino, I., Müller, J., Murguia-Flores, F., Naik, V., Niwa, Y., Noce, S., O'Doherty, S., Parker, R. J., Peng, C., Peng, S., Peters, G. P., Prigent, C., Prinn, R., Ramonet, M., Regnier, P., Riley, W. J., Rosentreter, J. A., Segers, A., Simpson, I. J., Shi, H., Smith, S. J., Steele, L. P., Thornton, B. F., Tian, H., Tohjima, Y., Tubiello, F. N., Tsuruta, A., Viovy, N., Voulgarakis, A., Weber, T. S., van Weele, M., van der Werf, G. R., Weiss, R. F., Worthy, D., Wunch, D., Yin, Y., Yoshida, Y., Zhang, W., Zhang, Z., Zhao, Y., Zheng, B., Zhu, Q., Zhu, Q., and Zhuang, Q.: The Global Methane Budget 2000–2017, Earth Syst. Sci. Data, 12, 1561–1623, https://doi.org/10.5194/essd-12-1561-2020, 2020.

Silyakova, A., Nomura, D., Kotovitch, M., Fransson, A., Delille, B., Chierici, M., and Granskog, M. A.: Methane release from open leads and new ice following an Arctic winter storm event, Polar Science, 33, 100874, https://doi.org/10.1016/j.polar.2022.100874, 2022.

Smith, S. D.: Coefficients for sea surface wind stress, heat flux, and wind profiles as a function of wind speed and temperature, J. Geophys. Res., 93, 15467, https://doi.org/10.1029/jc093ic12p15467, 1988.

Snoeijs-Leijonmalm and the the SAS-Oden 2021 Scientific Party: Expedition Report SWEDARCTIC: Synoptic Arctic Survey 2021 with icebreaker Oden urn:nbn:se:polar:diva-8882, 2022.

Spreen, G., Kaleschke, L., and Heygster, G.: Sea ice remote sensing using AMSR-E 89-GHz channels, J. Geophys. Res., 113, https://doi.org/10.1029/2005jc003384, 2008.

Thornton, B. F., Wik, M., and Crill, P. M.: Double-counting challenges the accuracy of high-latitude methane inventories, Geophys. Res. Lett., 43, https://doi.org/10.1002/2016gl071772, 2016a.

Thornton, B. F., Geibel, M. C., Crill, P. M., Humborg, C., and Mörth, C.-M.: Methane fluxes from the sea to the atmosphere across the Siberian shelf seas, Geophys. Res. Lett., 43, 5869–5877, https://doi.org/10.1002/2016gl068977, 2016b.

Thornton, B. F., Prytherch, J., Andersson, K., Brooks, I. M., Salisbury, D., Tjernström, M., and Crill, P. M.: Shipborne eddy covariance observations of methane fluxes constrain Arctic sea emissions, Sci. Adv., 6, https://doi.org/10.1126/sciadv.aay7934, 2020.

Tjernström, M., Birch, C. E., Brooks, I. M., Shupe, M. D., Persson, P. O. G., Sedlar, J., Mauritsen, T., Leck, C., Paatero, J., Szczodrak, M., and Wheeler, C. R.: Meteorological conditions in the central Arctic summer during the Arctic Summer Cloud Ocean Study (ASCOS), Atmos. Chem. Phys., 12, 6863–6889, https://doi.org/10.5194/acp-12-6863-2012, 2012.

Upstill-Goddard, R. C., Rees, A. P., and Owens, N. J. P.: Simultaneous high-precision measurements of methane and nitrous oxide in water and seawater by single phase equilibration gas chromatography, Deep Sea Research Part I: Oceanographic Research Papers, 43, 1669–1682, https://doi.org/10.1016/s0967-0637(96)00074-x, 1996.

Vachon, D., Prairie, Y. T., and Cole, J. J.: The relationship between near-surface turbulence and gas transfer velocity in freshwater systems and its implications for floating chamber measurements of gas exchange, Limnol. Oceanogr., 55, 1723–1732, https://doi.org/10.4319/lo.2010.55.4.1723, 2010.

Vüllers, J., Achtert, P., Brooks, I. M., Tjernström, M., Prytherch, J., Burzik, A., and Neely III, R.: Meteorological and cloud conditions during the Arctic Ocean 2018 expedition, Atmos. Chem. Phys., 21, 289–314, https://doi.org/10.5194/acp-21-289-2021, 2021.

Wanninkhof, R.: Relationship between wind speed and gas exchange over the ocean revisited, Limnol. Oceanogr. Methods, 12, 351–362, https://doi.org/10.4319/lom.2014.12.351, 2014.

Wanninkhof, R., Asher, W. E., Ho, D. T., Sweeney, C., and McGillis, W. R.: Advances in Quantifying Air-Sea Gas Exchange and Environmental Forcing, Annu. Rev. Mar. Sci., 1, 213–244, https://doi.org/10.1146/annurev.marine.010908.163742, 2009.

Weber, T., Wiseman, N. A., and Kock, A.: Global ocean methane emissions dominated by shallow coastal waters, Nat Commun, 10, https://doi.org/10.1038/s41467-019-12541-7, 2019.

Weiss, R. F.: Carbon dioxide in water and seawater: the solubility of a non-ideal gas, Marine Chemistry, 2, 203–215, https://doi.org/10.1016/0304-4203(74)90015-2, 1974.

Wiesenburg, D. A. and Guinasso, N. L., Jr.: Equilibrium solubilities of methane, carbon monoxide, and hydrogen in water and seawater, J. Chem. Eng. Data, 24, 356–360, https://doi.org/10.1021/je60083a006, 1979.

Woolf, D. K., Land, P. E., Shutler, J. D., Goddijn-Murphy, L. M., and Donlon, C. J.: On the calculation of air-sea fluxes of CO2in the presence of temperature and salinity gradients, J. Geophys. Res. Oceans, 121, 1229–1248, https://doi.org/10.1002/2015jc011427, 2016.

Yang, M., Prytherch, J., Kozlova, E., Yelland, M. J., Parenkat Mony, D., and Bell, T. G.: Comparison of two closed-path cavity-based spectrometers for measuring air–water CO2 and CH4 fluxes by eddy covariance, Atmos. Meas. Tech., 9, 5509–5522, https://doi.org/10.5194/amt-9-5509-2016, 2016.

Yasunaka, S., Murata, A., Watanabe, E., Chierici, M., Fransson, A., van Heuven, S., Hoppema, M., Ishii, M., Johannessen, T., Kosugi, N., Lauvset, S. K., Mathis, J. T., Nishino, S., Omar, A. M., Olsen, A., Sasano, D., Takahashi, T., and Wanninkhof, R.: Mapping of the air–sea CO2 flux in the Arctic Ocean and its adjacent seas: Basin-wide distribution and seasonal to interannual variability, Polar Science, 10, 323–334, https://doi.org/10.1016/j.polar.2016.03.006, 2016.

Yasunaka, S., Siswanto, E., Olsen, A., Hoppema, M., Watanabe, E., Fransson, A., Chierici, M., Murata, A., Lauvset, S. K., Wanninkhof, R., Takahashi, T., Kosugi, N., Omar, A. M., van Heuven, S., and Mathis, J. T.: Arctic Ocean CO2 uptake: an improved multiyear estimate of the air–sea CO2 flux incorporating chlorophyll a concentrations, Biogeosciences, 15, 1643–1661, https://doi.org/10.5194/bg-15-1643-2018, 2018.

		Bulk, with surface *pX*, *T*, *S*		Bulk, with 8 m *pX*, *T*, *S*	
Species, (unit)	**Measured**	**Ho et al., 2006**	**P&Y, 2021**	**Ho et al., 2006**	**P&Y, 2021**
CH_4 (μmol m^{-2} day^{-1})	3.5 ± 4.4	9.0 ± 8.2	6.4 ± 5.8	2.5 ± 3.7	1.8 ± 2.6
CO_2 (mmol m^{-2} day^{-1})	-7.3 ± 5.7	-12.9 ± 11.6	-9.1 ± 8.2	-7.3 ± 8.6	-5.1 ± 6.0

Table 1. Air-sea CH_4 and CO_2 Fluxes (mean ± standard deviation) determined from chamber measurements and from bulk methods using the specified gas transfer relationship and partial pressure, temperature and salinity measurement location.

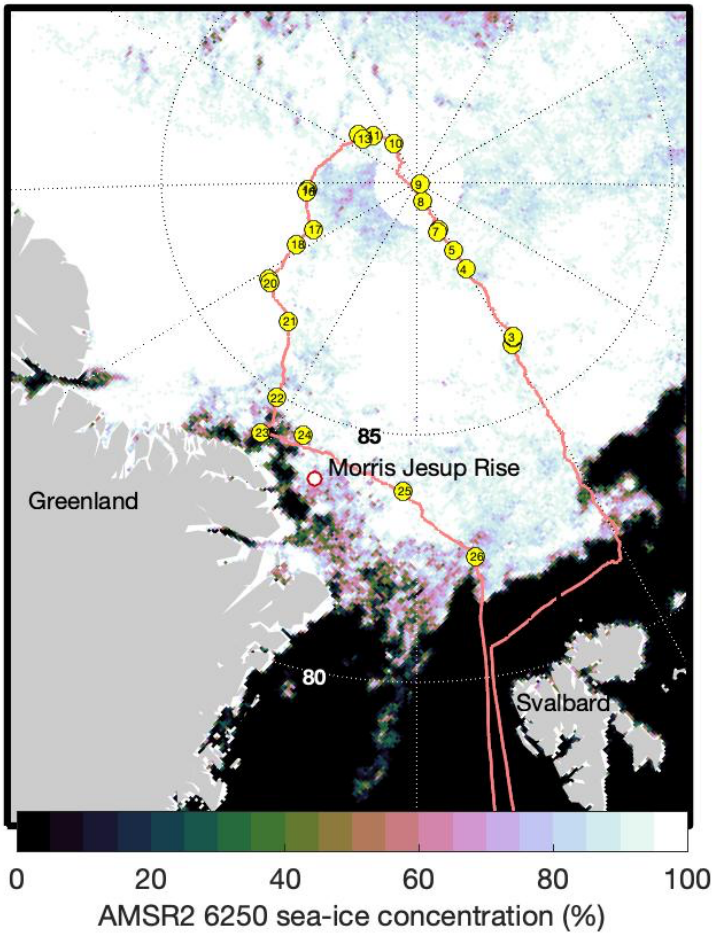

Figure 1. Map of the expedition route (red line) with chamber flux sampling locations (yellow circles) and numbers corresponding to Table S1. Sea-ice concentration is shown as determined for 2021-9-1 by AMSR-2 satellite observations and the ASI 6.25km^2 product.

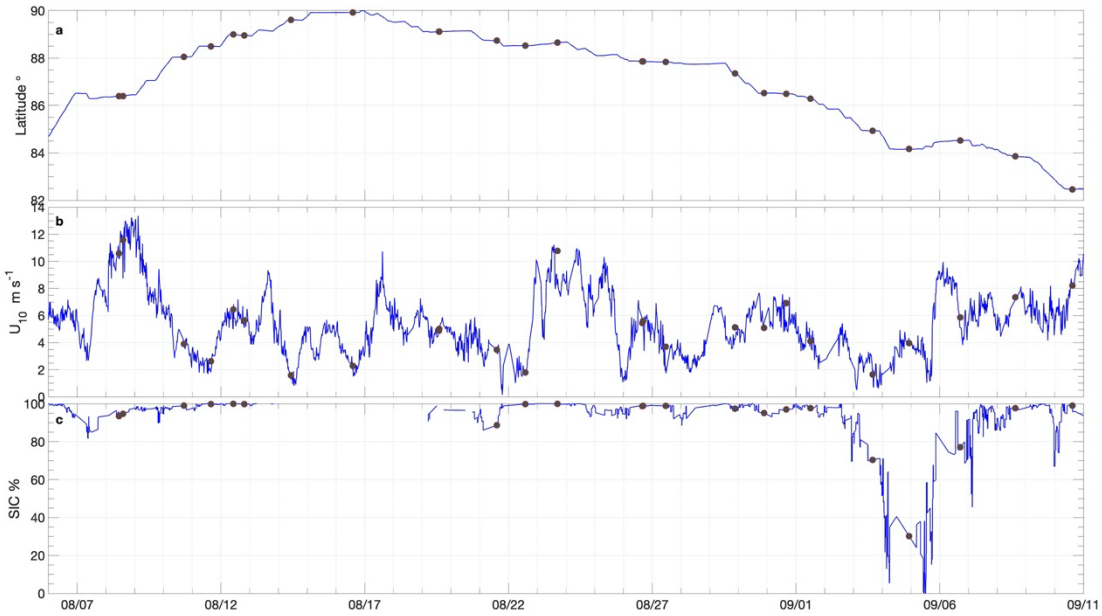

Figure 2. Time series of: a) *Oden's* latitude; b) wind speeds as measured on *Oden*; c) SIC determined from the ASI 6.25km^2 product interpolated to *Oden's* position. Grey circles in each plot show averaged values corresponding to the times of flux chamber measurement.

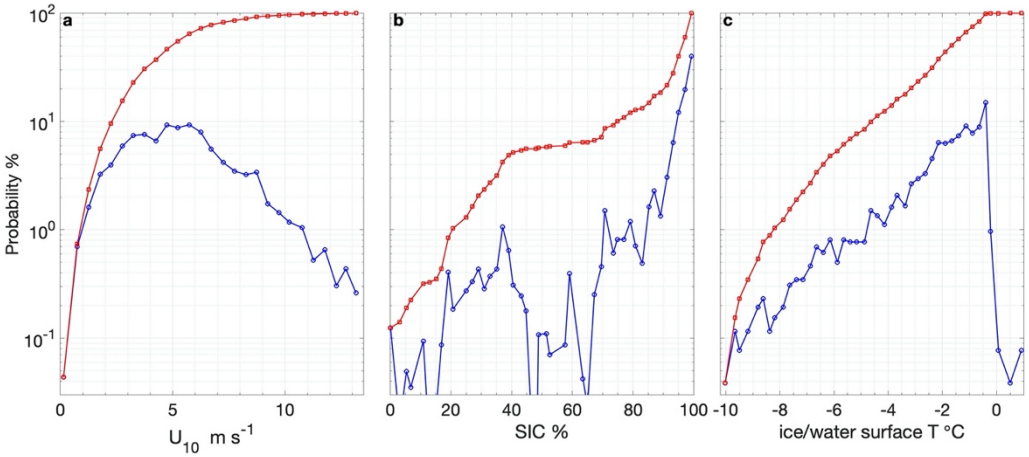

Figure 3. Occurrence probability (blue) and cumulative probability (red) during the expedition of a) wind speeds adjusted to 10 m height, b) SIC determined from the ASI 6.25km^2 product interpolated to *Oden's* position, c) surface ice or water temperature as measured with IR sensors onboard *Oden*.

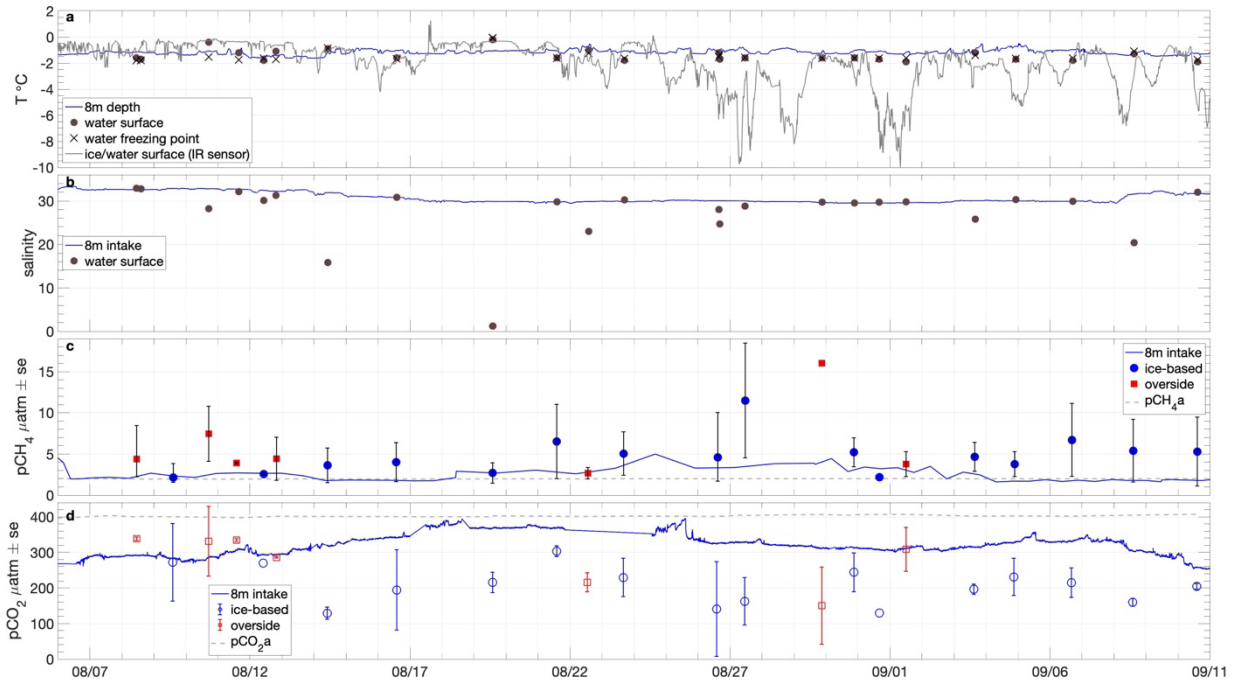

Figure 4. Time series of: a) seawater temperature at 8m depth and at the surface during chamber flux sampling, the corresponding freezing point determined from salinity measurement, and surface temperature (ice or water) measured from IR sensors onboard *Oden*; b) Salinity measured from the 8 m intake and at the surface during chamber flux sampling; c) partial pressures of CH_4 in water at specified depths and sampling locations and in the near-surface atmosphere; d) as per c for CO_2.

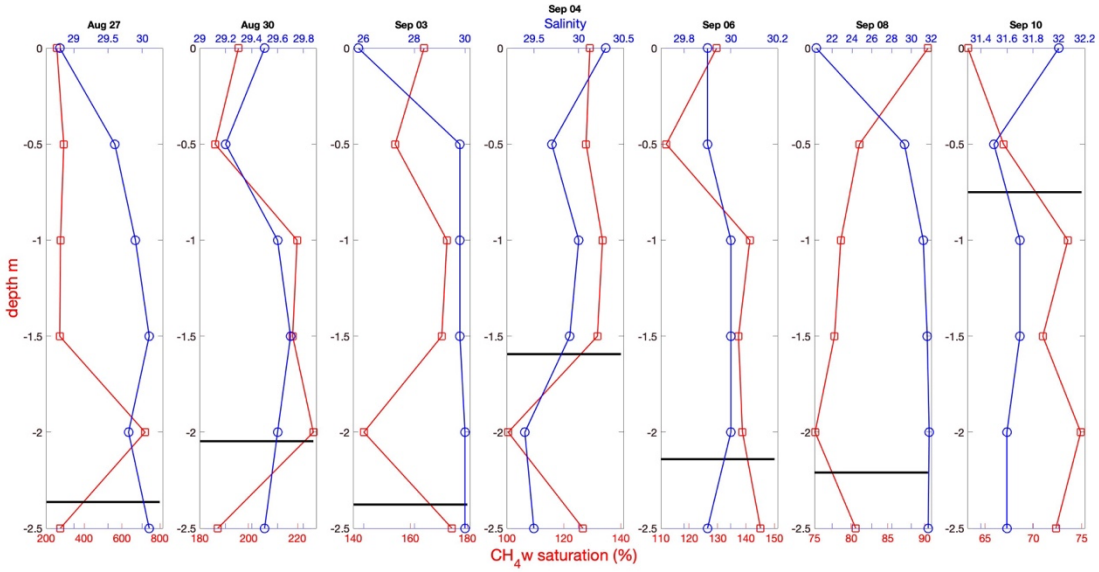

Figure 5. Near-surface profiles of CH_4 saturation (red) and salinity (blue) determined from ice-based Ruttner bottle sampling on the indicated day. An estimate of ice floe thickness is shown (thick black line), determined from auger drilling close to the sampling site.

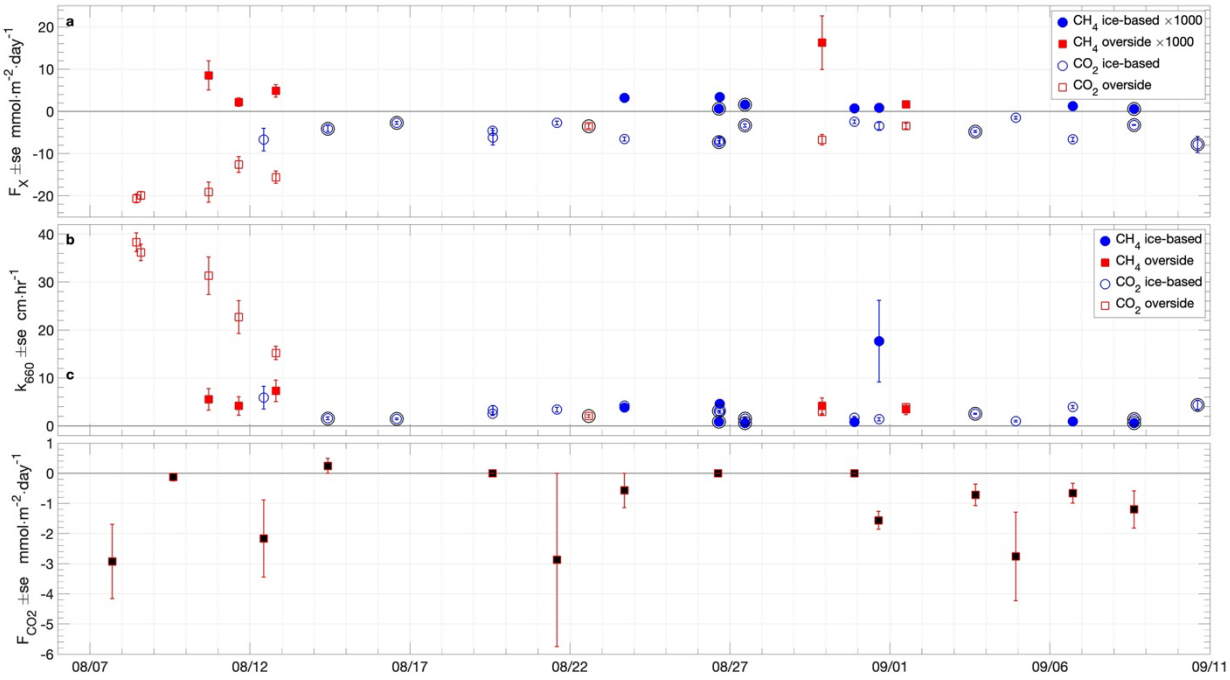

Figure 6. Time series of: a) air-sea fluxes of CH_4 (filled symbols) and CO_2 (non-filled symbols) measured with chamber flux systems at the specified sampling locations; b) k_{660} of CH_4 (filled symbols) and CO_2 (non-filled symbols) determined from air-sea chamber flux measurements using equations 1 and 2; c) snow-air CO_2 fluxes measured with the EGM-4 chamber flux system. Error bars are the standard error of the flux samples in each deployment. Outer black circles in a and b indicate measurements made in the presence of grease ice.

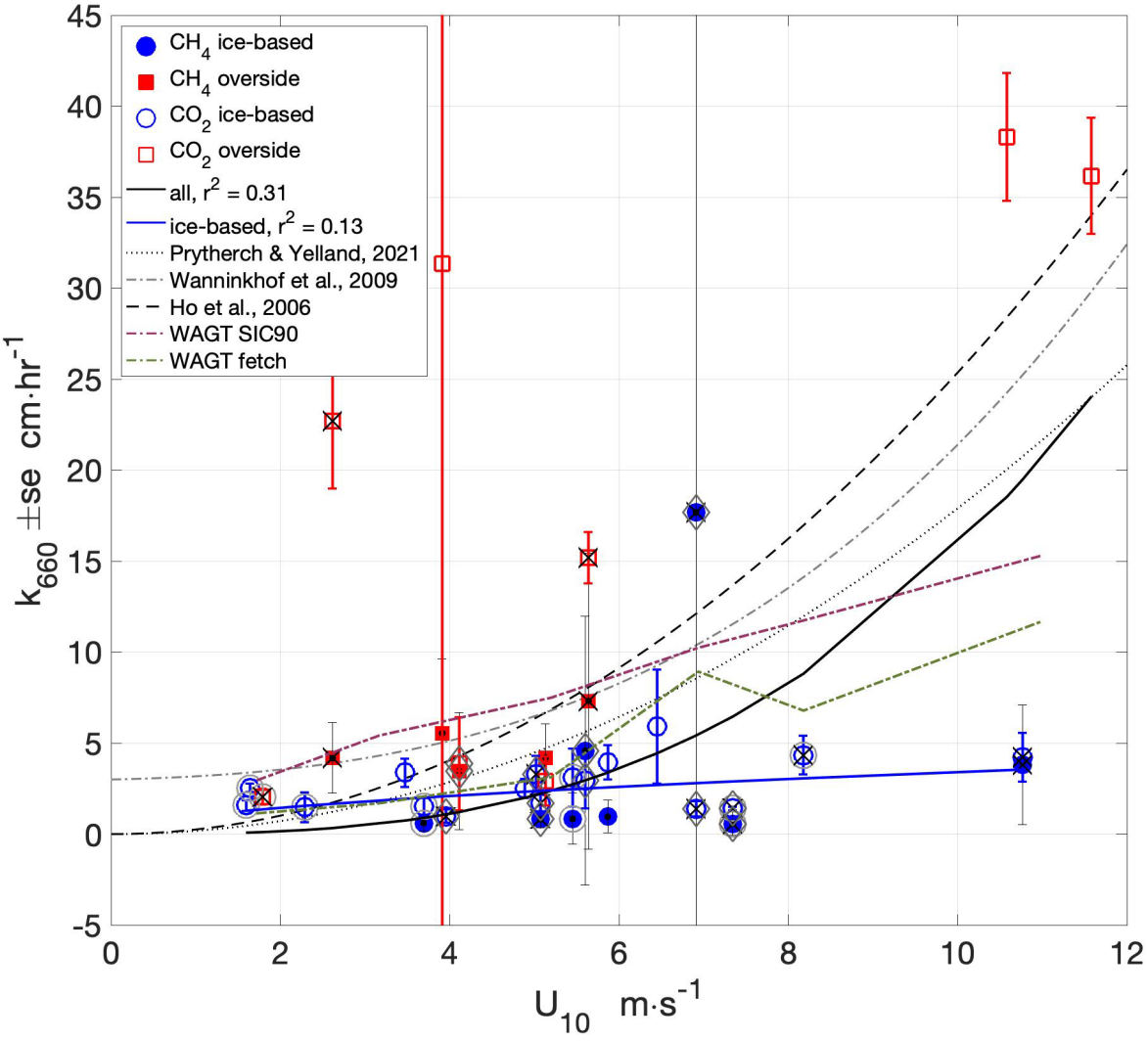

Figure 7. Wind speed dependence of k_{660} determined from air-sea chamber flux measurements using Eqs. (1) and (2), and non-linear least squares fits to the measurements ($y = a \times x^b$). Outer circles around the markers indicate measurements made in the presence of grease ice. Black crosses indicate measurements made with lead widths < 10 m. Diamonds indicate measurements made when surface buoyancy flux was negative (surface cooling). Also shown are three wind speed-based parameterisations of k_{660}. And the parametric WAGT model in both SIC mode (with SIC = 90%) and fetch mode using lead width.

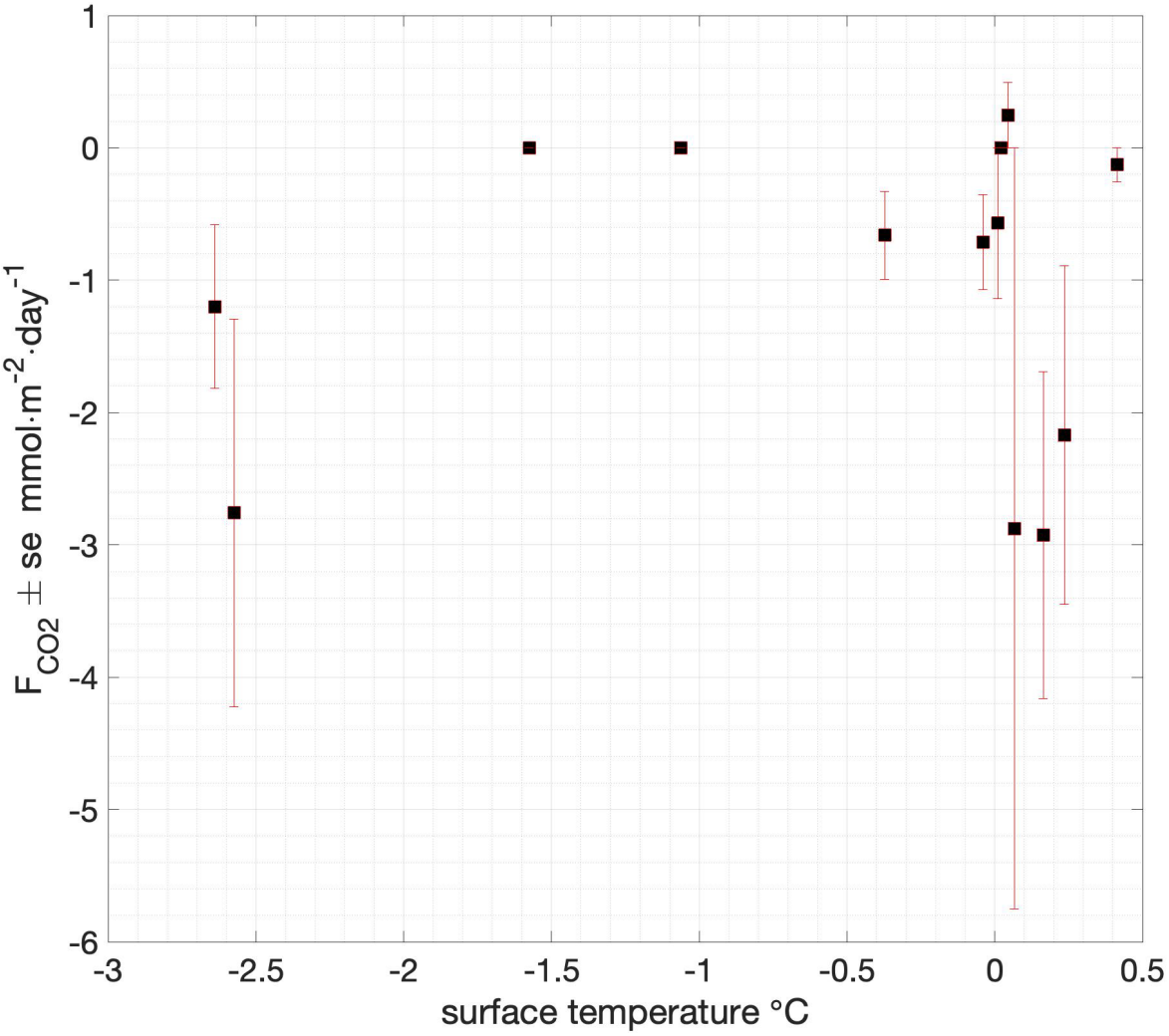

Figure 8. Surface temperature dependence of ice-air and snow-air CO_2 fluxes measured with the EGM-4 chamber flux system.

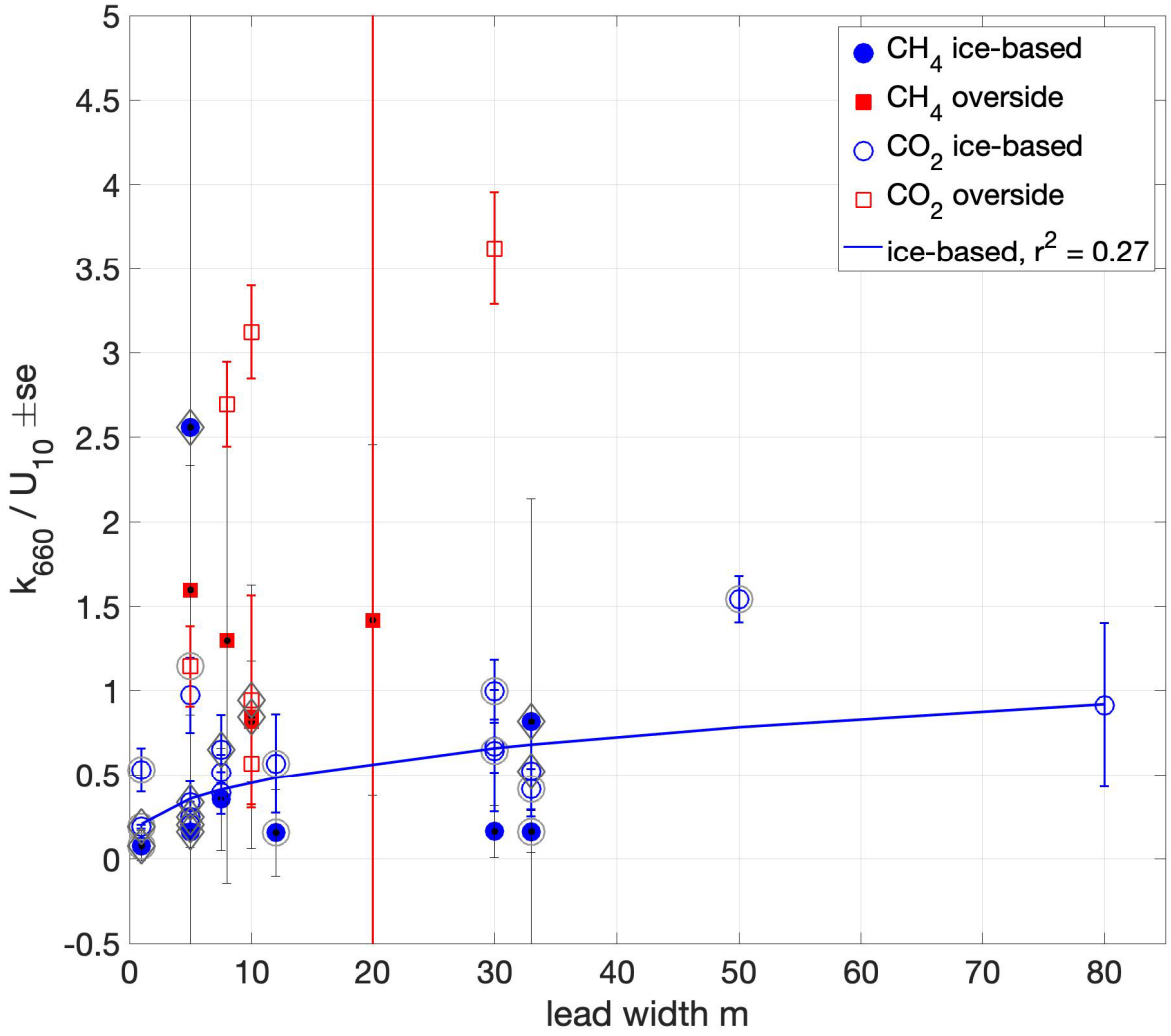

885

Figure 9. Dependence on lead width of water-air chamber flux-derived k_{660} normalised by U_{10}. A non-linear least squares fit to the ice-based measurements ($y = a \times x^b$) is shown (blue line). Outer circles around the markers indicate measurements made in the presence of grease ice. Diamonds indicate measurements made when surface buoyancy flux was negative (surface cooling).

890